



# Improved adaptive gaining-sharing knowledge algorithm with FDB-based guiding mechanism for optimization of optimal reactive power flow problem

Hüseyin Bakır<sup>1</sup> · Serhat Duman<sup>2</sup> · Ugur Guvenc<sup>3</sup> · Hamdi Tolga Kahraman<sup>4</sup>

Received: 14 February 2022 / Accepted: 8 March 2023 / Published online: 31 May 2023  
© The Author(s), under exclusive licence to Springer-Verlag GmbH Germany, part of Springer Nature 2023

## Abstract

Optimal reactive power flow (ORPF) is of great importance for the electrical reliability and economic operation of modern power systems. The integration of distributed generations (DGs) and two-terminal high voltage direct current (HVDC) systems into electrical networks has further complicated the ORPF problem. Due to the high computational complexity of the ORPF problem, a powerful and robust optimization algorithm is required to solve it. This paper proposes a powerful metaheuristic algorithm namely fitness-distance balance-based adaptive gaining-sharing knowledge (FDBAGSK). In the performance evaluation, 39 IEEE CEC benchmark functions are used to compare FDBAGSK with the original AGSK algorithm. Moreover, the proposed algorithm is applied to perform the ORPF task in modified IEEE 30- and IEEE 57-bus test systems. The effectiveness of the FDBAGSK method was tested for the optimization of three non-convex objectives: active power loss, voltage deviation and voltage stability index. The ORPF results obtained from the FDBAGSK algorithm are compared with other optimization algorithms in the literature. Given that all results are together, it has been observed that FDBAGSK is an effective method that can be used in solving global optimization and constrained real-world engineering problems.

**Keywords** Fitness distance balance-based adaptive gaining-sharing knowledge algorithm · Optimal reactive power flow · High voltage direct current · Distributed generations

## 1 Introduction

Optimal reactive power flow (ORPF) is a nonlinear, non-convex, and high-dimensional complex optimization problem. The main aim of the ORPF is to minimize a chosen objective function via optimal adjustment of control variables such as the voltage of generation buses, reactive power of capacitor banks, tap setting of transformers, etc. while satisfying various equality and inequality constraints [1]. Active power loss, voltage deviation, and voltage stability index are widely-used objective functions in the ORPF problem. The main reason behind it is that achieving these objectives means operating the electrical networks in an economical and stable manner [2, 3].

In today's world, ORPF has become one of the most important power system problems due to its critical role in the power industry. Power system researchers have used various optimization algorithms to deal with complex constraints and obtain feasible solutions to the non-linear ORPF problem. Ayan and Kılıç [4] used the artificial bee colony

---

✉ Hüseyin Bakır  
hbakir@dogus.edu.tr

Serhat Duman  
sduman@bandirma.edu.tr

Ugur Guvenc  
ugurguven@duzce.edu.tr

Hamdi Tolga Kahraman  
htolgakahraman@ktu.edu.tr

<sup>1</sup> Department of Electronics and Automation, Vocational School, Dogus University, Istanbul 34775, Türkiye

<sup>2</sup> Electrical Engineering, Engineering and Natural Sciences Faculty, Bandirma Onyedi Eylul University, Bandirma 10200, Türkiye

<sup>3</sup> Electrical and Electronics Engineering, Engineering Faculty, Duzce University, Duzce 81620, Türkiye

<sup>4</sup> Software Engineering of Technology Faculty, Karadeniz Technical University, Trabzon 61080, Türkiye

(ABC) algorithm to produce high-quality solutions to the ORPF problem. The success of the ABC in minimizing active power loss was evaluated using IEEE 30- and IEEE 118-bus test systems. The numerical results demonstrated that the ABC was able to achieve effective solutions for the ORPF problem. Yalçın and Arifoğlu [5] applied the genetic algorithm (GA) to the optimization of the ORPF problem in an IEEE 14-bus power system. Given that numerical results are together, it is observed that GA was more successful in solving the ORPF problem compared to its competitors. In another study, Moghadam and Seifi [6] dedicated on optimal reactive power planning problem. In this direction, the authors utilized the teaching–learning-based optimization (TLBO) method based on fuzzy logic to minimize power loss. The IEEE 30-bus test system results showed that the proposed algorithm can be a powerful alternative for solving the ORPF problem. Sulaiman et al. [7] investigated the best settings of control variables for reactive power flow problem. The authors applied the grey wolf optimizer (GWO) to solve the regarding problem. The efficiency of the algorithm has been tested in IEEE 30- and IEEE 118-bus power systems, and the GWO has outperformed other metaheuristics in terms of convergence speed and solution accuracy. Mehdinejad et al. [8] proposed the hybrid particle swarm optimization-imperialist competitive algorithm (PSO-ICA) for effective management of reactive power. The simulation results of IEEE 57- and IEEE 118-bus power systems demonstrated that the proposed hybrid approach had the ability to produce better-quality solutions than the ICA and PSO. Lenin et al. [9] used the hybrid tabu search-simulated annealing (HTSSA) algorithm to solve the ORPF problem. The effectiveness of HTSSA was evaluated in the IEEE-30 bus test system. The simulation results demonstrated that the HTSSA significantly reduced the active power loss. Mei et al. [10] applied the moth-flame optimization (MFO) algorithm to optimize the control variables of the ORPF problem. The performance of the algorithm has been tested in large-scale power systems, and it has been observed that the solution quality is better than its competitors. Sakr et al. [11] presented the differential evolution-based optimal reactive power optimization. The authors investigated the success of the proposed modified differential evolution algorithm (MDEA) in optimizing power loss and enhancing the voltage profile. Medani et al. [12] used the whale optimization algorithm (WOA) to optimize the control variables of the ORPF problem. The numerical results of the IEEE 14-, IEEE 30-, and Algerian 114-bus test systems revealed that the WOA is an efficient and robust method for solving the power system planning problem under study. Shaheen et al. [13] developed the hybrid improved marine predators algorithm and particle swarm optimization (IMPAPSO) method for the solution of the reactive power planning problem. The effectiveness of the proposed algorithm has been tested on IEEE 30-, IEEE 57- and IEEE

118-bus test systems. From the results, it has been seen that the convergence performance of the hybrid algorithm is superior to its competitors. Fadel et al. [14] employed the backtracking search algorithm (BSA) to find a feasible solution ORPF problem incorporating DGs and HVDC transmission systems. The effectiveness of the BSA was tested on modified IEEE 30- and 57-bus test systems with different cases. The simulation results showed that the power loss achieved by BSA was lower than its competitors in all test cases.

Based on the literature review, it can be said that the studies regarding the solution to the ORPF problem are a hot topic of interest to researchers. However, most of these studies investigated the classical ORPF. Contrary to the literature, the present research has centered on solving the AC/DC-ORPF problem in power systems that are modeled closest to the real world with the integration of DGs and HVDC systems. It is clear that power system researchers have applied a huge number of optimization algorithms to solve the ORPF problem. However, the obtained results have not been of the desired quality due to the drawbacks of optimization methods such as premature convergence and getting stuck in the local optima. From this point of view, a powerful and robust optimization algorithm is needed to provide results that improve upon the preceding ones. In this direction, this paper proposes a new metaheuristic algorithm, namely fitness-distance balance-based adaptive gaining-sharing knowledge (FDBAGSK).

A comprehensive scientific study has been carried out to test and verify the effectiveness of the proposed FDBAGSK algorithm. Firstly, it has been evaluated on 39 benchmark functions from CEC 2017 and CEC 2020, two of the most up-to-date test suites in the literature. The exploration, exploitation, and balanced search capabilities of the algorithm have been investigated by using unimodal, multimodal, hybrid, and composition-type problems in the relevant test suites. The data obtained from the experimental studies have been statistically analyzed using the Friedman and Wilcoxon tests. In addition, the convergence performance of the developed FDBAGSK has been validated by examining the boxplot graphs including the solution distribution span. After that, the developed FDBAGSK algorithm has been applied to the solution of nonlinear ORPF problem incorporating DGs and HVDC systems. Simulation studies have been performed on modified IEEE 30- and IEEE 57-bus test systems for optimization of power loss, voltage deviation, and voltage stability enhancement objectives.

The main contributions of this study can be listed as follows:

- A novel optimizer named fitness-distance balance-based adaptive gaining-sharing knowledge (FDBAGSK) is proposed.

- The exploration, exploitation, and balanced search abilities of the proposed FDBAGSK are tested by unimodal, multimodal, hybrid, and composition-type benchmark functions on CEC 2017 and CEC 2020 test suites. Furthermore, the convergence performance of the algorithm in 30, 50, and 100-dimensional search spaces was investigated.
- The practicability of FDBAGSK is evaluated for the optimization of the ORPF problem incorporating DGs and HVDC systems.
- The effectiveness of the proposed algorithm has been verified by Wilcoxon and Friedman statistical tests.

The remainder of the paper is organized as follows:

- **Section 2** presents the mathematical model of the ORPF incorporating DGs and HVDC systems.
- **Section 3** was prepared to introduce the design steps of the proposed FDBAGSK algorithm. In this direction, the fitness-distance balance (FDB) selection method, the basics of the original AGSK algorithm, and the proposed FDBAGSK algorithm are given, respectively.
- **Section 4** describes the experimental settings. It gives detailed information about the standards that were considered in executing the experimental studies and the benchmark problems used to test the performance of the algorithms.
- **Section 5** gives the findings and analysis results from the experimental studies.
- **Section 6** presents the conclusions of the study.

## 2 Mathematical model of ORPF problem incorporating DGs and HVDC systems

The optimal reactive power flow (ORPF) is a well-known power system problem in the field of the economical and reliable operation of electrical networks. The optimization of the ORPF problem is formulated as the minimizing chosen objective function such as active power loss, voltage deviation, and voltage stability index via adjustment of the control variables subject to various equality and inequality constraints [15, 16]. The mathematical model of the ORPF optimization problem is given in Eq. (1) [14, 17].

$$\begin{aligned} &\text{minimize } F_{\text{obj}}(M, P) \\ &\text{subject to } g(M, P) = 0 \\ &\quad h(M, P) \leq 0 \end{aligned} \tag{1}$$

where  $F_{\text{obj}}$  is the objective function,  $M$  and  $P$  represent the state and control variables,  $g(M, P)$  and  $h(M, P)$  are the equality and inequality constraints, respectively. This study

has focused on the formulation and solution of the AC/DC-ORPF problem involving DGs and HVDC systems.

### 2.1 State variables

The state variables of the AC/DC-ORPF problem incorporating DGs and HVDC systems are given in Eq. (2) [14].

$$\begin{aligned} M &= [M^{AC}, M^{DC}] \\ M^{AC} &= [P_{THG_1}, Q_{THG_1} \dots Q_{THG_{NTHG}}, V_{L_1} \dots V_{L_{NPQ}}] \\ M^{DC} &= [t_r, t_i, \alpha_r, \gamma_i, v_{dr}, v_{di}] \end{aligned} \tag{2}$$

where  $Q_{THG_1}$  represents reactive power of thermal generators,  $P_{THG_1}$  is the active power of the swing generator,  $V_L$  shows the voltage value of the load buses.  $NTHG$  and  $NPQ$  are the number of thermal generators and load buses.  $t_r$  and  $t_i$  display the tap ratio of transformers at the rectifier and inverter sides, respectively. The excitation angle of the rectifier and inverter are symbolized by  $\alpha_r$  and  $\gamma_i$ .  $v_{dr}$  and  $v_{di}$  represent the DC voltage of the rectifier and inverter terminals, respectively.

### 2.2 Control variables

The control variables of the ORPF problem incorporating DGs and HVDC systems can be listed as follows [14]:

$$\begin{aligned} P &= [P^{AC}, P^{DC}] \\ P^{AC} &= [P_{THG_2} \dots P_{THG_{NTHG}}, V_{THG_1} \dots V_{THG_{NTHG}}, \\ &\quad T_1 \dots T_{NT}, P_{DG_1} \dots P_{DG_{NDG}}, loc_{DG_1} \dots loc_{DG_{NDG}}] \\ P^{DC} &= [P_r, P_i, Q_r, Q_i, i_d] \end{aligned} \tag{3}$$

where  $P_{THG}$  represents the thermal generator active power (except for the swing generator),  $V_{THG}$  is the voltage value of the generator buses, and  $T$  indicates the tap ratio of transformers.  $P_{DG}$  and  $loc_{DG}$  show the active power output and location of the DG, respectively.  $NTHG$ ,  $NT$ , and  $NDG$  represent number of thermal generators, transformers, and distributed generations, respectively.  $P_r$ ,  $P_i$ ,  $Q_r$ , and  $Q_i$  are the active and reactive power output of the rectifier and inverter, and  $i_d$  is the direct current.

### 2.3 Objective functions

In this study, active power loss, voltage deviation and  $L$ -index objective functions are optimized. The mathematical model of objective functions is explained in the following subsections.

### 2.3.1 Active power loss

The active power loss objective function can be formulated as given in Eq. (4) [14].

$$F_{obj}(M, P) = F_{obj1} = P_{loss} = \sum_{k=1}^{NTHG} P_{THGk} + \sum_{k=1}^{NDG} P_{DGk} - \sum_{k=1}^{N_{bus}} P_{Lk} \quad (4)$$

where  $P_{THGk}$  is the generator active power at bus  $k$ ,  $P_{DGk}$  represents the active power of the distributed generator connected to the  $k$ -th bus,  $P_{Lk}$  denotes load demand at bus  $k$ , and  $N_{bus}$  represents the total bus number.

### 2.3.2 Voltage deviation

In modern power systems, the bus voltage deviation is considered one of the most important security indices. Because a small change in voltage can affect the entire system and cause a power outage [18, 19]. The voltage deviation objective function can be written as follows [20]:

$$F_{obj}(M, P) = F_{obj2} = VD = \sum_{i=1}^{NPQ} |VL_i - 1| \quad (5)$$

where  $VD$  represents the voltage deviation value,  $NPQ$  is the number of load buses, and  $VL_i$  shows  $i$ -th load bus voltage.

### 2.3.3 Enhancement of voltage stability

Voltage stability is a major problem in modern power systems and usually results from a change in power system configuration, increased load on the load buses, or a disturbance in the power systems. The  $L$ -index value of the load buses is a powerful indicator of voltage stability [20]. The  $L$ -index parameter is expected to take values between 0 and 1, with 0 defining a no-load case, and 1 defining voltage collapse. For modern power systems, a lower  $L$ -index value corresponds to a more stable status [21, 22].

$$L_j = \left| 1 - \sum_{i=1}^{NTHG} F_{ji} \frac{V_i}{V_j} \right| \quad j = 1, 2, \dots, NPQ \quad (6)$$

$$F_{ji} = -[Y_{LL}]^{-1}[Y_{LG}] \quad (7)$$

where  $L_j$  is the  $L$ -index value of the  $j$ -th load bus, and  $Y_{LL}$  and  $Y_{LG}$  sub-matrices are calculated from the bus admittance matrix ( $Y_{BUS}$ ) after separating the load and generator buses, as defined in Eq. (8) [18, 23].

$$\begin{bmatrix} I_L \\ I_G \end{bmatrix} = [Y_{BUS}] \begin{bmatrix} V_L \\ V_G \end{bmatrix} = \begin{bmatrix} Y_{LL} & Y_{LG} \\ Y_{GL} & Y_{GG} \end{bmatrix} \begin{bmatrix} V_L \\ V_G \end{bmatrix} \quad (8)$$

The maximum value of the  $L$ -index is defined as the objective function (Eq. 9) [20]:

$$F_{obj}(M, P) = F_{obj3} = \min(L_{max}) = \min(\max(L_j)) \quad (9)$$

## 2.4 Equality constraints

This sub-section introduces the equality constraints of the AC/DC-ORPF optimization problem.

### 2.4.1 AC system equality constraints

The AC bus model including DGs and HVDC systems is shown in Fig. 1. The active and reactive power equations of the  $k$ -th AC bus can be defined as follows [14]:

$$P_{THGk} + P_{DGk} - P_{Lk} - P_{Dk} - P_k = 0 \quad (10)$$

$$Q_{THGk} + Q_{Ck} - Q_{Lk} - Q_{Dk} - Q_k = 0 \quad (11)$$

where  $P_{THGk}$ ,  $P_{DGk}$ ,  $P_{Lk}$ ,  $P_{Dk}$ , and  $P_k$  are defined as an active power of the thermal generator, distributed generation, load bus, DC link, and  $k$ -th bus;  $Q_{THGk}$ ,  $Q_{Ck}$ ,  $Q_{Lk}$ ,  $Q_{Dk}$ , and  $Q_k$  are defined as reactive power of the thermal generator, shunt compensator, load bus, DC link, and  $k$ -th bus, respectively.

The active and reactive power transferred from the  $k$ -th bus to the AC system can be defined as follows [20, 22]:

$$P_k = v_k \sum_{j=1}^{N_{bus}} v_j [G_{kj} \cos(\delta_k - \delta_j) + B_{kj} \sin(\delta_k - \delta_j)] \quad (12)$$

$$Q_k = v_k \sum_{j=1}^{N_{bus}} v_j [G_{kj} \sin(\delta_k - \delta_j) - B_{kj} \cos(\delta_k - \delta_j)] \quad (13)$$

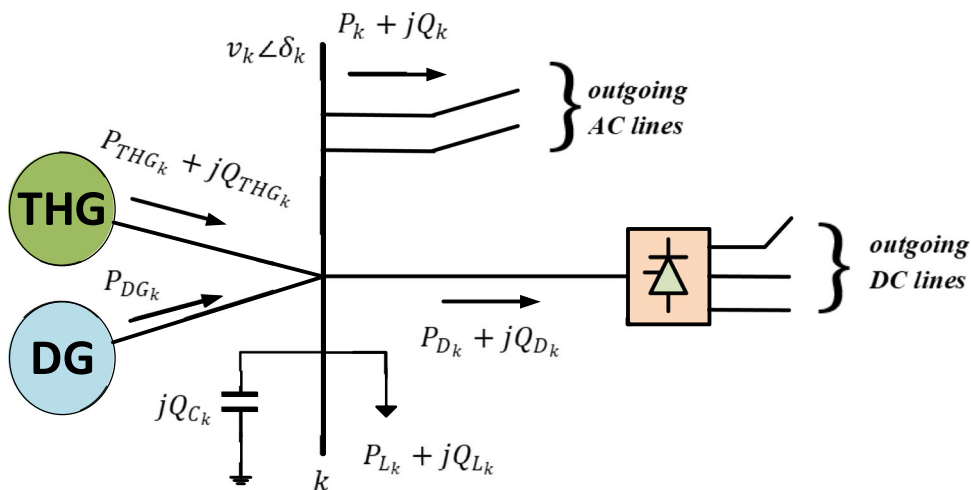
where  $v_k$  and  $v_j$  denote the voltage magnitude at bus  $k$  and  $j$ , respectively.  $G_{kj}$  and  $B_{kj}$  are conductance and susceptance,  $\delta_k$  and  $\delta_j$  depict the voltage angle of  $k$ -th and  $j$ -th bus, respectively.

If the rectifier and inverter losses are ignored, the power equations of the rectifier and inverter attached to the AC bus can be written as follows [14, 20]:

$$P_{Dk} = P_r \quad (14)$$

$$Q_{Dk} = Q_r \quad (15)$$

**Fig. 1** AC bus model incorporating DGs and HVDC transmission systems



$$P_{Dk} = -P_i \tag{16} \quad v_{di} = v_{doi} \cos \gamma - r_{ci} i_d \Rightarrow r_{ci} = \frac{3x_{ci}}{\pi} \tag{24}$$

$$Q_{Dk} = Q_i \tag{17} \quad P_i = v_{di} i_d \tag{25}$$

**2.4.2 DC system equality constraints**

The schematic diagram of the two-terminal HVDC transmission system is depicted in Fig. 2. In the figure,  $v_r, v_i, i_r,$  and  $i_i$  denote the AC voltage values and currents of the rectifier and inverter, respectively.  $\delta_r, \delta_i, \xi_r,$  and  $\xi_i$  show the phase and AC current angles at the rectifier and inverter side [20, 22]. The equations of the rectifier side can be formulated as follows [24–26]:

$$v_{dor} = k t_r v_r \Rightarrow k = \frac{3\sqrt{2}}{\pi} \tag{18} \quad \phi_i = \cos^{-1}(v_{di}/v_{doi}) \tag{26}$$

$$v_{dr} = v_{dor} \cos \alpha - r_{cr} i_d \Rightarrow r_{cr} = \frac{3x_{cr}}{\pi} \tag{19} \quad Q_i = |P_i \tan \phi_i| \tag{27}$$

$$P_r = v_{dr} i_d \tag{20}$$

$$\phi_r = \cos^{-1}(v_{dr}/v_{dor}) \tag{21}$$

$$Q_r = |P_r \tan \phi_r| \tag{22}$$

where  $v_{dor}$  denotes the rectifier open circuit DC voltage value.  $r_{cr}$  and  $\phi_r$  are the commutating resistance and phase angle at the rectifier side, respectively.

The inverter side equations can be written as follows [24–26]:

$$v_{doi} = k t_i v_i \Rightarrow k = \frac{3\sqrt{2}}{\pi} \tag{23}$$

where  $v_{doi}$  denotes the inverter open circuit DC voltage value.  $r_{ci}$  and  $\phi_i$  are the commutating resistance and phase angle at the inverter side, respectively. The equivalent circuit of a two-terminal HVDC transmission system is illustrated in Fig. 3. Considering the DC-link resistance, the voltage balance of the DC system can be written as follows [14]:

$$v_{dr} - v_{di} - r_{dc} i_d = 0 \tag{28}$$

**2.5 Inequality constraints**

In this sub-section, inequality constraints of the AC/DC-ORPF problem are given.

**2.5.1 AC system inequality constraints**

AC system inequality constraints can be formulated by Eqs. (29–34).

$$P_{THGi}^{min} \leq P_{THGi} \leq P_{THGi}^{max} \forall i \in N_{THG} \tag{29}$$

$$P_{DGi}^{min} \leq P_{DGi} \leq P_{DGi}^{max} \forall i \in N_{DG} \tag{30}$$

$$Q_{THGi}^{min} \leq Q_{THGi} \leq Q_{THGi}^{max} \forall i \in N_{THG} \tag{31}$$

**Fig. 2** Two-terminal HVDC transmission system

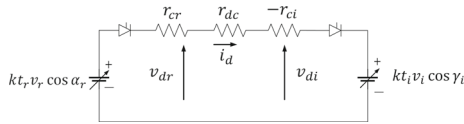
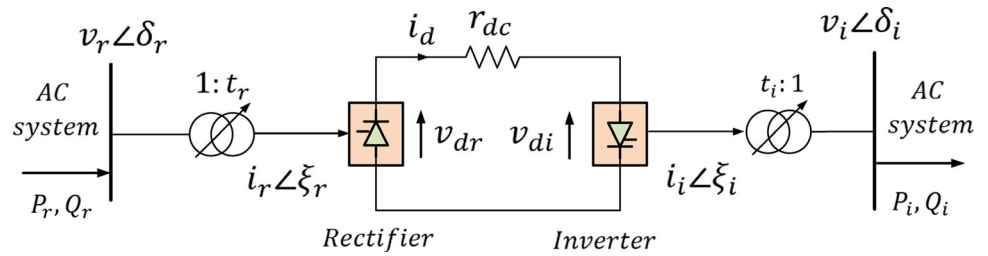


**Fig. 3** Two-terminal HVDC system equivalent model

$$V_{THGi}^{min} \leq V_{THGi} \leq V_{THGi}^{max} \forall i \in NTHG \tag{32}$$

$$V_{Li}^{min} \leq V_{Li} \leq V_{Li}^{max} \forall i \in NPQ \tag{33}$$

$$T_i^{min} \leq T_i \leq T_i^{max} \forall i \in NT \tag{34}$$

**2.5.2 DC system inequality constraints**

DC system inequality constraints are given in Eqs. (35–41).

$$i_d^{min} \leq i_d \leq i_d^{max} \tag{35}$$

$$P_{Dk}^{min} \leq P_{Dk} \leq P_{Dk}^{max} k = i, r \tag{36}$$

$$Q_{Dk}^{min} \leq Q_{Dk} \leq Q_{Dk}^{max} k = i, r \tag{37}$$

$$t_k^{min} \leq t_k \leq t_k^{max} k = i, r \tag{38}$$

$$v_{dk}^{min} \leq v_{dk} \leq v_{dk}^{max} k = i, r \tag{39}$$

$$\alpha_r^{min} \leq \alpha_r \leq \alpha_r^{max} \tag{40}$$

$$\gamma_i^{min} \leq \gamma_i \leq \gamma_i^{max} \tag{41}$$

The fitness function of the AC/DC-ORPF problem incorporating DGs and HVDC systems can be formulated as in Eq. (42). In that equation,  $F_{obj}(M, P)$  represents the objective function that include active power loss ( $F_{obj1}$ ), voltage deviation ( $F_{obj2}$ ), and voltage stability enhancement ( $F_{obj3}$ ).

$$J_{fitness} = F_{obj}(M, P) + Penalty$$

$$Penalty = \lambda_1 (P_{THG1} - P_{THG1}^{lim})^2$$

$$\begin{aligned}
 & + \lambda_2 \sum_{i=1}^{NTHG} (Q_{THGi} - Q_{THGi}^{lim})^2 \\
 & + \lambda_3 \sum_{i=1}^{NPQ} (V_{Li} - V_{Li}^{lim})^2 + \lambda_4 (t_r - t_r^{lim})^2 \\
 & + \lambda_5 (t_i - t_i^{lim})^2 + \lambda_6 (\alpha_r - \alpha_r^{lim})^2 \\
 & + \lambda_7 (\gamma_i - \gamma_i^{lim})^2 + \lambda_8 (v_{dr} - v_{dr}^{lim})^2 \\
 & + \lambda_9 (v_{di} - v_{di}^{lim})^2
 \end{aligned} \tag{42}$$

where  $\lambda_1, \lambda_2, \lambda_3, \lambda_4, \lambda_5, \lambda_6, \lambda_7, \lambda_8,$  and  $\lambda_9$  are penalty factor terms. If the value of the state variables is lower or higher than the limit values, the value of these variables is set to the limit. Constraint violation states are given in the following equations:

$$P_{THG1}^{lim} = \begin{cases} P_{THG1}^{min} & \text{if } P_{THG1} < P_{THG1}^{min} \\ P_{THG1}^{max} & \text{if } P_{THG1} > P_{THG1}^{max} \end{cases} \tag{43}$$

$$Q_{THGi}^{lim} = \begin{cases} Q_{THGi}^{min} & \text{if } Q_{THGi} < Q_{THGi}^{min} \\ Q_{THGi}^{max} & \text{if } Q_{THGi} > Q_{THGi}^{max} \end{cases} \tag{44}$$

$$V_{Li}^{lim} = \begin{cases} V_{Li}^{min} & \text{if } V_{Li} < V_{Li}^{min} \\ V_{Li}^{max} & \text{if } V_{Li} > V_{Li}^{max} \end{cases} \tag{45}$$

$$t_r^{lim} = \begin{cases} t_r^{min} & \text{if } t_r < t_r^{min} \\ t_r^{max} & \text{if } t_r > t_r^{max} \end{cases} \tag{46}$$

$$t_i^{lim} = \begin{cases} t_i^{min} & \text{if } t_i < t_i^{min} \\ t_i^{max} & \text{if } t_i > t_i^{max} \end{cases} \tag{47}$$

$$\alpha_r^{lim} = \begin{cases} \alpha_r^{min} & \text{if } \alpha_r < \alpha_r^{min} \\ \alpha_r^{max} & \text{if } \alpha_r > \alpha_r^{max} \end{cases} \tag{48}$$

$$\gamma_i^{lim} = \begin{cases} \gamma_i^{min} & \text{if } \gamma_i < \gamma_i^{min} \\ \gamma_i^{max} & \text{if } \gamma_i > \gamma_i^{max} \end{cases} \tag{49}$$

$$v_{dr}^{lim} = \begin{cases} v_{dr}^{min} & \text{if } v_{dr} < v_{dr}^{min} \\ v_{dr}^{max} & \text{if } v_{dr} > v_{dr}^{max} \end{cases} \tag{50}$$

$$v_{di}^{lim} = \begin{cases} v_{di}^{min} & \text{if } v_{di} < v_{di}^{min} \\ v_{di}^{max} & \text{if } v_{di} > v_{di}^{max} \end{cases} \tag{51}$$

### 3 Method

Although MHS algorithms differ from each other in several ways, there are two search tasks common to all of them [27–30]. The first task is exploitation, which refers to the ability to perform a neighborhood search around a reference location. This task, also known as *fine-tuning*, can be easily fulfilled by MHS algorithms because there are simple and effective mathematical methods that are well known for searching around a reference location [31, 32]. The second task is exploration, which refers to the algorithm’s ability to efficiently research the entire search space. In contrast to exploitation, exploration is challenging because there are an unlimited number of solutions to be investigated in search space. Exploration is a process performed to eliminate local solution traps and plays a major role in determining the algorithm search performance [33–35]. The existence of many local solution traps in complex search spaces causes MHS algorithms to get caught in local solution traps while performing their exploration tasks and thus leads to premature convergence [36]. To overcome these problems, the MHS algorithm must have strong exploration and balanced search capability. The present study has centered on improving the exploration and balanced search capabilities of the AGSK algorithm, which suffers from premature convergence. In this direction, the guide selection strategy of the AGSK algorithm was redesigned using the FDB selection method. Thus, the FDBAGSK algorithm, which has the ability to effectively explore the search space and converge to the global optimum successfully, was developed. The next sub-sections introduce the FDB selection method, optimization model of the AGSK, and the proposed FDBAGSK algorithm.

#### 3.1 Fitness-distance balance (FDB) selection method

Fitness-distance balance (FDB) [37] is an effective and powerful selection method developed by Kahraman et al. in 2020. The fundamentals of FDB method are based on the selection of guides with high potential to improve the quality of the search process. Although FDB is relatively similar to the greedy selection method, the most important feature that distinguishes FDB from the greedy approach is that the solution candidates are selected according to their scores. The FDB method considers two criteria to calculate the scores of the solution candidates: the fitness value and the distance to the best solution ( $x_{best}$ ) in the population [37, 38]. This ensures that the solution candidate with the high fitness value is selected and also prevents the selection of a solution candidate that is very close to the  $x_{best}$  [33]. In order to calculate the FDB scores of solution candidates in a  $P$ -population, the following steps should be applied [37, 39]:

**Step 1:** Assume that  $x_i$  ( $i = 1, 2, \dots, k$ ) represents individual in population  $P$ . Accordingly, the population includes

$k$  individuals (solution candidates) and each individual  $x_i$  is represented by  $x_{ij} = [x_{i1}, x_{i2}, \dots, x_{in}]$ , where  $n$  is the design variables number and  $f_i$  ( $i = 1, 2, \dots, k$ ) is the fitness value. In light of these definitions,  $P$  and  $FV$  vectors are created as shown in Eq. (52).

$$P \equiv \begin{bmatrix} x_{11} & \cdots & x_{1n} \\ \vdots & \ddots & \vdots \\ x_{k1} & \cdots & x_{kn} \end{bmatrix}_{k \times n}, \quad FV = \begin{bmatrix} f_1 \\ \cdot \\ \cdot \\ \cdot \\ f_k \end{bmatrix}_{k \times 1} \tag{52}$$

**Step 2:** The Euclidean distance value between  $i$ -th individual ( $x_i$ ) and  $x_{best}$  is calculated by Eq. (53), where  $x_{best}$  refers to the individual with the best fitness value.

$$\begin{aligned} & \forall_{i=1}^k x_i \neq x_{best}, D_{x,i} \\ & = \sqrt{(x_{i[1]} - x_{best[1]})^2 + (x_{i[2]} - x_{best[2]})^2 + \dots + (x_{i[n]} - x_{best[n]})^2} \end{aligned} \tag{53}$$

**Step 3:** The distance vector  $D_x$  is represented by Eq. (54).

$$D_x \equiv \begin{bmatrix} d_1 \\ \cdot \\ \cdot \\ \cdot \\ d_k \end{bmatrix}_{k \times 1} \tag{54}$$

**Step 4:** The FDB selection method evaluates individuals according to their scores. The score value is calculated using the normalized fitness value ( $normFV$ ) and normalized distance value ( $normD_x$ ) of individuals. Normalized values are used in order to prohibit the dominance of fitness and distance values in the score calculation. The weight coefficient ( $w$ ) determines the effect of  $FV$  and  $D_x$  in the FDB score calculation of the individuals. In this study, the effects of fitness and distance values on score calculation were considered equal ( $w = 0.5$ ).

$$\forall_{i=1}^k x_i, S_{x[i]} = w * normFV_{x[i]} + (1 - w) * normD_{x[i]} \tag{55}$$

**Step 5:** The score vector of the population  $P$  is represented by Eq. (56).

$$S_x \equiv \begin{bmatrix} s_1 \\ \cdot \\ \cdot \\ \cdot \\ s_k \end{bmatrix}_{k \times 1} \tag{56}$$

In the FDB selection method, individuals that will guide the search process are chosen based on the  $S_x$  vector shown in Eq. (56). For detailed information about the FDB selection method, please review Ref. [37].

the search-process lifecycle, the search for a global optimum is carried out through exploration and exploitation operators. Finally, the population  $P$  is updated based on the fitness value of the individuals.

---

**Algorithm 1.** General steps of the GSK optimization process

---

```

1. Initialization
2.  $P$ : Create initial population randomly as specified in Eq. (52)
3. for  $i=1: k$  (number of individuals) do
4.    $FV$ : Evaluate the fitness for each individual as given in Eq. (52)
5. end
6. while search process lifecycle: up to termination criteria do
7.   Step 1: Selection
8.     Select individuals from  $P(x_{i-1}, x_{i+1}, x_r, x_{pbest}, x_m, x_{pworst})$ 
9.   Step 2: Search (Exploration and Exploitation)
10.    Junior Gaining Sharing Knowledge Phase ( $x_{i-1}, x_{i+1}, x_r$ )
11.    Senior Gaining Sharing Knowledge Phase ( $x_{pbest}, x_m, x_{pworst}$ )
12.   Step 3: Update
13.     Update the  $P$ -population based on the fitness value of individuals
14. end

```

---

### 3.2 Overview of AGSK algorithm

Adaptive gaining-sharing knowledge (AGSK) [40] is a powerful metaheuristic algorithm developed by Mohamed et al. in 2020. The AGSK has been developed to provide an effective algorithm that can solve difficult optimization problems with rapid convergence and high solution accuracy by enhancing the search capability of the gaining-sharing knowledge (GSK) [41] algorithm. The strength of the AGSK is in its dynamic adaptation of the knowledge factor ( $k_f$ ) and knowledge ratio ( $k_r$ ). The AGSK algorithm was created by combining the GSK with the adaptive procedure. The basics of the GSK algorithm and the adaptive procedure are introduced in the following subsections.

#### 3.2.1 Gaining-sharing knowledge algorithm

GSK is a population-based algorithm inspired by the behavior of people to acquire and share knowledge throughout their lives. It is based on two crucial stages: junior gaining-sharing knowledge and senior gaining-sharing knowledge [41].

As given in Algorithm 1 (please see lines 6–14), the GSK optimization process consists of three steps: selection, search, and update. In the selection step, the individuals who will guide the search process are identified. The GSK algorithm uses sequential, random, and greedy selection methods to identify guide solution candidates. In the second step of

As in other metaheuristic algorithms, GSK uses the initial population  $P$  to start the optimization process. The  $P$  is created based on  $k$  solution candidates called individuals and  $n$  design parameters. The  $FV$  vector represents the fitness value of the individuals, and it is created as given in Eq. (52). For the junior and senior gaining-sharing knowledge stages, the dimension of design variables ( $n$ ) is calculated by Eq. (57) [40, 41].

$$n_{Gained\_Shared\_Junior} = n * \left(1 - \frac{FEs}{maxFEs}\right)^K \quad (57)$$

$$n_{Gained\_Shared\_Senior} = n - n_{Gained\_Shared\_Junior}$$

where  $FEs$  and  $maxFEs$  are the current and maximum function evaluation scores, respectively. The dimension of the design parameter to be updated using the junior stage initially takes its maximum value, and over time, the number of dimensions to be updated using the senior stage increases. The speed of learning and sharing knowledge increases at some points in the human lifetime and decreases at others. This dynamic process is simulated by setting the information rate  $K$  in Eq. (57). Due to the heterogeneous distribution of the population, parameter  $K$  takes a random value in the range [0–1] for half of the population individuals and an integer value in the range [1–20] for the other half [40, 41].

In the junior gaining-sharing knowledge stage, knowledge resources are limited, so each individual tends to obtain information only from the closest family members and relatives.

Eq. (58). Knowledge is shared with a randomly selected individual  $x_r$  from the population. The pseudo-code of the junior gaining-sharing knowledge phase is given in Algorithm 2.

**Algorithm 2.** Junior gaining-sharing knowledge phase [40, 41]

```

1. for i=1: k do
2.     for j=1: n do
3.         if rand<=kr (knowledge ratio) then
4.             if f(xi) > f(xr) then
5.                 xijnew = xi + kf [(xi-1 - xi+1) + (xr - xi)]
6.             else
7.                 xijnew = xi + kf [(xi-1 - xi+1) + (xi - xr)]
8.             end if
9.         else
10.            xijnew = xijold
11.        end if
12.    end for
13. end for
    
```

Individuals are updated via the following steps [40, 41]:

**Step 1:** Individuals are ranked in descending order according to fitness values as shown in Eq. (58). In that equation,  $x_{best}$  and  $x_{worst}$  represent the individuals with the best and worst fitness values, respectively.

$$P = \begin{bmatrix} x_{best} \\ \vdots \\ x_{i-1} \\ x_i \\ x_{i+1} \\ \vdots \\ x_{worst} \end{bmatrix}_{k \times n} \tag{58}$$

**Step 2:** The  $x_{i-1}$  (closest better) and  $x_{i+1}$  (closest worse) are identified for each individual ( $x_i, i = 1, 2, \dots, k$ ) using

At the senior gaining-sharing knowledge stage, individuals have excellent capability to gain and share knowledge from their wide networks of friends, social media, and books. This stage examines the effects of individuals classified as the best and worst on the other individuals. Thus, individuals are updated via the following steps [41]:

**Step 1:** The population is divided into three categories considering the rank given in Eq. (58). Accordingly, the first 100p% individuals are in the best-category, the last 100p% individuals are in the worst-category, and the other individuals  $k-(2 \times 100p\%)$  are in the better/middle category.

**Step 2:** For each  $x_i$ , two random vectors ( $x_{pbest}$  and  $x_{pworst}$ ) are selected for gaining knowledge. Then,  $x_m$  is then selected from the better/middle individual category for sharing knowledge. The percentage of the best and worst categories is determined by  $p$ , with its value in the range of [0,1].  $p$  was considered as a 0.1. The pseudo-code of the senior gaining-sharing knowledge phase is presented in Algorithm 3.

**Algorithm 3.** Senior gaining-sharing knowledge phase [40, 41]

---

```

1. for i=1: k do
2.   for j=1: n do
3.     if rand<=kr (knowledge ratio) then
4.       if f(xi) > f(xm) then
5.         xijnew = xi + kf [(xpbest - xpworst) + (xm - xi)]
6.       else
7.         xijnew = xi + kf [(xpbest - xpworst) + (xi - xm)]
8.       end if
9.     else
10.      xijnew = xijold
11.    end if
12.  end for
13. end for

```

---

**3.2.2 Adaptive procedure**

The search performance of the AGSK is directly related to the success of the junior and senior gaining-sharing knowledge stages, where exploration and exploitation tasks are fulfilled. The knowledge factor ( $k_f$ ) and knowledge ratio ( $k_r$ ) are accountable for managing the junior and senior gaining-sharing phases during the search process. For this, the  $k_f$  and  $k_r$  parameters should be dynamically adjusted to meet the requirements of the search process.  $k_f$  determining the total knowledge number to be transferred from others to the  $i$ -th individual and  $k_r$  denoting the ratio between the present and acquired experience. The value of  $k_f$  is greater than 1 and that of  $k_r$  is between 0 and 1 [40]. The pseudo-code of the adaptation scheme is presented in Algorithm 4.

**Algorithm 4.** Adaptation scheme [40]

---

```

1. Begin
2.   Initialize parameter setting pool ( $k_f$  and  $k_r$ ), and  $Kw\_P$ 
3.   while  $FES < maxFES$ 
4.     if  $FES > 0.1 * maxFES$  then
5.       Update  $Kw\_P$ 
6.     end if
7.     For each individual determine one setting based on  $Kw\_P$ 
8.     Produce new individuals ( $x_i^{new}$ )
9.     Evaluate  $x_i^{new}$  and update  $FES$ 
10.    Check out the development for each setting  $\Delta_{ps}$ 
11.  end while
12. end for
13. end

```

---

In the AGSK algorithm, an adaptive process is used to determine the ideal value of the  $k_f$  and  $k_r$  parameters. The predetermined parameter settings for the pool vectors in AGSK were  $k_f = [0.1 \ 1 \ 0.5 \ 1]$  and  $k_r = [0.2 \ 0.1 \ 0.9 \ 0.9]$ . As shown in Algorithm 4 line 5, when the condition  $FES > 0.1 * maxFES$  is satisfied, the  $Kw\_P$  probability parameter is

updated using Eq. (61). According to the probability parameter, the  $k_f$  and  $k_r$  values are assigned from the parameter pool for each individual [41].

$$w_{ps} = \sum_{i=1}^p f(x_i^{new}) - f(x_i^{old}) \quad (59)$$

$$\Delta_{ps} = \max\left(0.05, \frac{w_{ps}}{\text{sum}(w_{ps})}\right) \quad (60)$$

$$Kw\_P_{g+1} = (1 - c)Kw\_P_g + c\Delta_{ps} \quad (61)$$

where  $w_{ps}$  represents the sum of the differences between the old and new fitness values for each individual belonging to the parameter setting.  $f$  is the fitness function,  $x_i^{new}$  and  $x_i^{old}$  are defined as new and old individuals, respectively.  $p$  is the number of individuals belonging to the parameter set-

ting.  $\Delta_{ps}$  represents the improvement rate for each parameter setting, and  $c$  is the learning rate.

The population size is updated in every generation to increase the search performance of the AGSK. The population size is reduced gradually using Eq. (62).

**Table 1** Mathematical model of the proposed FDBAGSK

Cases	Explanation	Mathematical model of FDBAGSK variants
Case-1	In the senior gaining-sharing knowledge phase, $x_{FDB}$ is used instead of the $x_m$ vector	$x_{ij}^{new} = x_i + k_f [(x_{pbest} - x_{pworst}) + (x_{FDB} - x_i)] \quad (63)$ $x_{ij}^{new} = x_i + k_f [(x_{pbest} - x_{pworst}) + (x_i - x_{FDB})] \quad (64)$
Case-2	In the senior gaining-sharing knowledge phase, $x_{FDB}$ is used instead of the $x_{pworst}$ vector	$x_{ij}^{new} = x_i + k_f [(x_{pbest} - x_{FDB}) + (x_{FDB} - x_i)] \quad (65)$ $x_{ij}^{new} = x_i + k_f [(x_{pbest} - x_{FDB}) + (x_i - x_{FDB})] \quad (66)$
Case-3	In the junior gaining-sharing knowledge phase, $x_{RFDB}$ was used instead of $x_{i+1}$ vector, and $x_{FDB}$ was used instead of $x_r$ vector	$x_{ij}^{new} = x_i + k_f [(x_{i-1} - x_{RFDB}) + (x_{FDB} - x_i)] \quad (67)$ $x_{ij}^{new} = x_i + k_f [(x_{i-1} - x_{RFDB}) + (x_i - x_{FDB})] \quad (68)$
Case-4	In the junior gaining-sharing knowledge phase, $x_{RFDB}$ was used instead of $x_{i-1}$ vector, and $x_{FDB}$ was used instead of $x_r$ vector	$x_{ij}^{new} = x_i + k_f [(x_{RFDB} - x_{i+1}) + (x_{FDB} - x_i)] \quad (69)$ $x_{ij}^{new} = x_i + k_f [(x_{RFDB} - x_{i+1}) + (x_i - x_{FDB})] \quad (70)$
Case-5	In the junior gaining-sharing knowledge phase, $x_{FDB}$ is used instead of the $x_r$ vector	$x_{ij}^{new} = x_i + k_f [(x_{i-1} - x_{i+1}) + (x_{FDB} - x_i)] \quad (71)$ $x_{ij}^{new} = x_i + k_f [(x_{i-1} - x_{i+1}) + (x_i - x_{FDB})] \quad (72)$

$$k_{g+1} = round \left[ \left( \frac{popsize_{min} - popsize_{init}}{maxFEs} \right) FE_s + popsize_{init} \right] \quad (62)$$

where  $k_{g+1}$  is the population size in the next generation. The initial value of the population size is  $popsize_{init} = 40 * n$ , and the minimum value is  $popsize_{min} = 12$  [41].

### 3.3 Proposed FDBAGSK algorithm

This sub-section introduces the design steps of the proposed FDBAGSK algorithm. First, the FDBAGSK variants created by applying the FDB method and their mathematical models are introduced. Subsequently, the pseudo-code of the proposed method is given.

The strength of the AGSK algorithm is that it provides adaptive settings for the knowledge factor ( $k_f$ ) and knowledge ratio ( $k_r$ ) control parameters. However, the results of experimental studies conducted in 30/50/100 dimensions using unimodal, multimodal, hybrid, and composition type problems in the CEC 2017 and CEC 2020 test suites revealed that the AGSK converged prematurely, and its exploitation-exploration balance was insufficient. The poor exploration of the algorithm was the main reason for its premature convergence, especially in multimodal-type problems containing many local solution traps. The AGSK was insufficient to provide the balance of exploration and exploitation required to successfully research the complex search spaces of hybrid and composition type problems. To eliminate these problems, we decided to strengthen the exploration and

balanced search capabilities of the algorithm using the FDB selection method. To this end, the guide selection strategy in the AGSK was re-designed using the FDB selection method.

The FDBAGSK variants (Case-1, ..., Case-5) created by applying the FDB-based guide mechanism are given in Table 1. In the Case-1 and Case-2 variants, the FDB method was applied to the senior gaining-sharing knowledge stage. The Case-1 variant was designed by using the  $x_{FDB}$  instead of the  $x_m$  solution candidate in the  $i$ -th solution candidate update equations specified in Algorithm 3, lines 5 and 7. In Case-2, the  $x_{pworst}$  solution candidate in the same equations was replaced by the  $x_{FDB}$  solution candidate determined via the FDB method. Case-3, Case-4, and Case-5 are FDBAGSK variants in which the FDB method was applied to the junior gaining-sharing knowledge stage of the AGSK algorithm. In these three variants, the solution candidate update equations given in Algorithm 2, lines 5 and 7 were revised. Case-3 was designed using  $x_{RFDB}$  instead of the solution candidate  $x_{i+1}$ , and  $x_{FDB}$  instead of the solution candidate  $x_r$ . In Case-4, it was suggested that two different solution candidates should be selected by FDB-based methods. Here, whereas the  $x_{i-1}$  solution candidate was selected by the FDB roulette method ( $x_{RFDB}$ ), the  $x_r$  solution candidate was identified by the FDB ( $x_{FDB}$ ). The other FDB variant (Case-5) was designed using  $x_{FDB}$  instead of  $x_r$  in the junior gaining-sharing knowledge phase. The above-mentioned  $x_{FDB}$  and  $x_{RFDB}$  refer to the solution candidates selected by the greedy method (i.e., the solution candidates with the highest scores) and the roulette method, according to the score value given in Eq. (56), respectively. The pseudo-code of the FDBAGSK optimization method is given in Algorithm 5.

**Algorithm 5.** Pseudo-code of proposed FDBAGSK algorithm

```

1. Initialize parameters ( $maxFES$ ,  $k_f$ ,  $k_r$ ,  $K$ ,  $p$ ,  $Kw\_P$ )
2. Create initial  $P$ -population of  $k$  solution candidates ( $x_i$ ,  $i=1,2,\dots,k$ )
3. for  $i=1:k$ 
4.  $FV$ : evaluate the fitness value of the solution candidates
5. end
6. while  $FES < maxFES$  do
7.   if  $FES > 0.1 * maxFES$  then
8.     Adaptive process (Algorithm 4)
9.   end if
10.  Calculate the gaining-sharing dimensions for junior and senior phases (Eq. 57)
11.  // Selection Stage //
12.  Select individuals from  $P$  ( $x_{i-1}, x_{i+1}, x_r, x_{pbest}, x_m, x_{pworst}$ )
13.  FDB selection method
14.  for  $i=1:k$  do
15.    Calculate the Euclidean distance between  $x_i$  and  $x_{best}$  using Eq. (53)
16.    Calculate FDB score for each solution candidate ( $x_i$ ) using Eq. (55)
17.  end for
18.  Determine  $x_{FDB}$  and  $x_{RFDB}$  based on the score value ( $S_x$ ) given in Eq. (56)
19.  // Search Stage -Exploration and Exploitation //
20.  //Junior gaining-sharing knowledge phase //
21.  for  $i=1:k$  do
22.    for  $j=1:n$  do
23.      if  $rand \leq k_r$  (knowledge ratio) then
24.        //Case 3//
25.        if  $f(x_i) > f(x_r)$  then
26.           $x_{ij}^{new} = x_i + k_f [(x_{i-1} - x_{RFDB}) + (x_{FDB} - x_i)]$  //Eq. (67) //
27.        else
28.           $x_{ij}^{new} = x_i + k_f [(x_{i-1} - x_{RFDB}) + (x_i - x_{FDB})]$  //Eq. (68) //
29.        end if
30.        //Case 4//
31.        if  $f(x_i) > f(x_r)$  then
32.           $x_{ij}^{new} = x_i + k_f [(x_{RFDB} - x_{i+1}) + (x_{FDB} - x_i)]$  //Eq. (69) //
33.        else
34.           $x_{ij}^{new} = x_i + k_f [(x_{RFDB} - x_{i+1}) + (x_i - x_{FDB})]$  //Eq. (70) //
35.        end if
36.        //Case 5//
37.        if  $f(x_i) > f(x_r)$  then
38.           $x_{ij}^{new} = x_i + k_f [(x_{i-1} - x_{i+1}) + (x_{FDB} - x_i)]$  //Eq. (71) //
39.        else
40.           $x_{ij}^{new} = x_i + k_f [(x_{i-1} - x_{i+1}) + (x_i - x_{FDB})]$  //Eq. (72) //
41.        end if
42.        else
43.           $x_{ij}^{new} = x_{ij}^{old}$ 
44.        end if
45.      end for
46.    end for
47.  //Senior gaining-sharing knowledge phase //
48.  for  $i=1:k$  do
49.    for  $j=1:n$  do
50.      if  $rand \leq k_r$  (Knowledge ratio) then
51.        //Case 1//
52.        if  $f(x_i) > f(x_m)$  then
53.           $x_{ij}^{new} = x_i + k_f [(x_{pbest} - x_{pworst}) + (x_{FDB} - x_i)]$  //Eq. (63) //
54.        else
55.           $x_{ij}^{new} = x_i + k_f [(x_{pbest} - x_{pworst}) + (x_i - x_{FDB})]$  //Eq. (64) //
56.        end if
57.        //Case 2//
58.        if  $f(x_i) > f(x_m)$  then
59.           $x_{ij}^{new} = x_i + k_f [(x_{pbest} - x_{FDB}) + (x_{FDB} - x_i)]$  //Eq. (65) //

```

```

60.         else
61.              $x_{ij}^{new} = x_i + k_f [(x_{pbest} - x_{FDB}) + (x_i - x_{FDB})]$  //Eq. (66)//
62.         end if
63.     else
64.          $x_{ij}^{new} = x_{ij}^{old}$ 
65.     end if
66. end for
67. end for
68. // Update Stage //
69. if  $f(x_i^{new}) \leq f(x_i^{old})$  then
70.      $x_i^{old} = x_i^{new}$ ,  $f(x_i^{old}) = f(x_i^{new})$ 
71. end if
72. if  $f(x_i^{new}) \leq f(x_{best}^g)$  then
73.      $x_{best}^g = x_i^{new}$ ,  $f(x_{best}^g) = f(x_i^{new})$ 
74. end if
75. end while
76. return  $x_{best}$ 

```

## 4 Experimental settings

Comprehensive experimental studies were carried out to test and validate the search performance of the AGSK and FDBAGSK variants. Different problem types and complex search spaces were considered to scrutinize the exploitation, exploration, and balanced search capabilities of MHS algorithms. In order to objectively compare the search performance of MHS algorithms, the following conditions were applied.

- The effectiveness of the algorithms is tested on 39 benchmark functions of CEC 2017 and CEC 2020 test suites.
- For a fair comparison, all MHS algorithms use 1000\*Dimension maximum function evaluations (*maxFEs*) as search process termination criteria.
- The search performance of the algorithms was tested using different problem types: unimodal, multimodal, hybrid, and composition problems.
- Experiments were carried out in 30, 50, and 100 dimensions to examine the behavior of the optimization algorithms in low/middle/high-dimensional search spaces.
- 51 independent runs were conducted to obtain robust data for statistical analysis. Nonparametric pairwise Wilcoxon [42] and Friedman [43] tests were used for statistical analysis. The Wilcoxon test was done at a 5% significance level.
- All experimental studies were done using MATLAB R2016a on an Intel(R) Core (TM) i5-1135G7 @2.40 GHz X64-processor with a 16 GB RAM computer.

Table 2 provides information about the CEC test suites used in the experimental studies.

## 5 Results and analysis

This section gives the results of two experimental studies in the field of optimization. The first subsection analyses the search performance of FDBAGSK in CEC global optimization problems. The second sub-section presents the simulation results of the nonlinear ORPF optimization problem.

### 5.1 Determining the best FDBAGSK version on global optimization problems

This sub-section presents a comparative analysis of the original AGSK and the FDBAGSK variants on the CEC 2017 and CEC 2020 benchmark problems.

#### 5.1.1 Statistical analysis

In the experimental studies, 39 benchmark test functions were used to test and validate the search performance of six algorithms (AGSK and five FDBAGSK variants). For detailed information on the FDBAGSK variants, please review sub-Sect. 3.3. *Proposed FDBAGSK algorithm*. Each test function was run 51 times in order to obtain statistically robust data. Additionally, the experiments were performed in 30, 50, and 100 dimensions to analyze the convergence performance of the algorithms depending on the dimension change. Using the nonparametric Friedman and Wilcoxon tests, 35,802 (39\*6\*51\*3) data items were statistically analyzed.

A comparative analysis of the FDBAGSK versions (Case-1, ..., Case-5) and the base AGSK was performed, and the best FDB-based version was determined by using the Friedman test. Table 3 presents the Friedman test results of the AGSK

**Table 2** Benchmark suites used in the experimental studies

Title	Number of test functions	Function types	Search range	Dimension
CEC 2017 [44]	29	Unimodal Multimodal Hybrid	[− 100, 100]	30, 50 and 100
CEC 2020 [45]	10	Composition		

**Table 3** Friedman test ranking of AGSK and FDBAGSK variants

Algorithms	Dimension = 30		Dimension = 50		Dimension = 100		Mean rank
	CEC 2017	CEC 2020	CEC 2017	CEC 2020	CEC 2017	CEC 2020	
	Case-1	<b>2.87</b>	<b>2.93</b>	<b>2.73</b>	<b>2.71</b>	<b>2.98</b>	
Case-2	3.45	3.35	3.41	3.12	3.32	2.94	3.26
Case-3	3.35	3.35	3.44	3.59	3.40	3.54	3.44
Case-4	3.35	3.34	3.54	3.77	3.44	3.73	3.52
Case-5	3.70	3.62	3.72	3.53	3.51	3.70	3.63
AGSK	4.25	4.37	4.13	4.25	4.33	4.28	4.26

Bold values show the best Friedman score

and FDBAGSK variants. In order to determine the best FDBAGSK variant, thirty-six experiments were carried out in 30, 50, and 100 dimensions. The Friedman ranking of competitive algorithms was determined based on the *Mean Rank* index, which considers the average of all experiments and is presented in the last column of Table 3. As can be seen clearly from the table, the FDB-based algorithms outperformed the original AGSK in all experiments. Admittedly, among the FDBAGSK variants, Case-1 is the most successful.

Wilcoxon pairwise comparison test results for the original AGSK and the FDBAGSK variants are given in Table 4. The results showed that the FDBAGSK variants exhibited a better search performance than the AGSK algorithm for all dimensions in both benchmark test suites. The performance of the Case-1 (20/9/0) and Case-4 (20/8/1) variants on the CEC 2017 test problems for 30 dimensions was pretty close. Moreover, for the experiments in the same test suite, the search performance of Case-1 (17/11/1) and Case-2 (21/6/2) was better than their competitors in the 50 and 100 dimensions, respectively. For the experiments in the CEC2020 test suite, the performance of the Case-1 (8/2/0) in 30 and 50 dimensions and the Case-2 (8/2/0) variant in 100 dimensions was better compared to its competitors. Given that all results are together, it is observed that the FDB-based variants outperformed the original AGSK algorithm in all experiments.

Table 5 discusses the search performance of the algorithms for unimodal, multimodal, hybrid, and composition benchmark functions in both the CEC 2017 and CEC 2020 test suites. In Table 5, the best Friedman rank obtained for each

experiment is marked in bold. The results given in the relevant table clearly show that the FDBAGSK variants achieved a better ranking than the basic AGSK algorithm in all experiments. A plus point is that the AGSK algorithm gave a worse search performance than its competitors in the four different problem types. This indicates that the main handicap of the AGSK algorithm is the premature convergence problem. The underlying reason behind it can be attributed to the inability of the AGSK algorithm to effectively imitate the process in nature. In order to eliminate this problem, the use of the FDB selection method is a feasible solution, as it was designed with reference to nature. The results given in Table 5, clearly show that the search performance of the FDBAGSK versions improved by the FDB method.

Table 6 gives the error statistics for the AGSK and the FDBAGSK variants in the 30-, 50-, and 100-dimensional experiments. In the relevant table, each cell includes mean and standard deviation values, respectively. For each test function, the best value obtained in the regarding dimension is marked in bold. Additionally, the data were interpreted with the box plots prepared to facilitate an understanding of the search performance of the algorithms. The box plots show the minimum, maximum, and mean/standard deviation error values achieved by the algorithms for 51 independent runs. Figures 4 and 5 illustrate box plots in 30, 50, and 100 dimensions for unimodal, multimodal, hybrid, and composition type benchmark functions selected from the CEC 2017 and CEC 2020 test suites.

Figure 4 illustrates the box-plot graphs in 30/50/100 dimensions for the F1 unimodal, F5 multimodal, F18 hybrid, and F21 composition-type test functions of the CEC 2017

**Table 4** Wilcoxon pairwise comparison results for AGSK and FDBAGSK variants

vs. AGSK + / = / -	Dimension = 30		Dimension = 50		Dimension = 100	
	CEC 2017	CEC 2020	CEC 2017	CEC 2020	CEC 2017	CEC 2020
Case-1	20/9/0	8/2/0	17/11/1	8/2/0	18/5/6	7/2/1
Case-2	15/11/3	5/5/0	13/14/2	6/4/0	21/6/2	8/2/0
Case-3	15/14/0	6/4/0	14/14/1	3/7/0	15/13/1	4/5/1
Case-4	20/8/1	5/5/0	12/15/2	3/7/0	19/9/1	5/4/1
Case-5	15/12/2	5/5/0	12/15/2	5/4/1	15/12/2	3/6/1

**Table 5** Friedman ranking of AGSK and FDBAGSK variants for unimodal, multimodal, hybrid, and composition problems

Function type			AGSK	Case-1	Case-2	Case-3	Case-4	Case-5
CEC 2017	Unimodal	D = 30	4.06	3.25	<b>3.06</b>	3.48	3.59	3.56
		D = 50	4.28	3.32	3.48	<b>3.19</b>	3.48	3.25
		D = 100	4.71	<b>2.87</b>	3.50	3.18	3.73	3.00
	Multimodal	D = 30	4.41	<b>2.20</b>	3.39	3.29	3.72	3.98
		D = 50	4.48	<b>2.09</b>	3.32	3.38	3.73	4.00
		D = 100	4.48	<b>2.06</b>	3.35	3.41	3.76	3.94
	Hybrid	D = 30	4.12	<b>3.08</b>	3.48	3.30	3.24	3.78
		D = 50	3.92	<b>3.09</b>	3.43	3.50	3.44	3.62
		D = 100	4.25	<b>3.05</b>	3.12	3.55	3.31	3.73
	Composition	D = 30	4.15	<b>3.01</b>	3.60	3.49	3.24	3.52
		D = 50	4.03	<b>2.64</b>	3.42	3.52	3.59	3.80
		D = 100	4.16	3.45	3.46	3.35	3.35	<b>3.23</b>
CEC 2020	Unimodal	D = 30	5.51	4.45	<b>2.18</b>	2.86	2.57	3.43
		D = 50	5.90	4.20	3.67	2.45	2.71	<b>2.08</b>
		D = 100	5.86	4.12	4.06	2.06	3.43	<b>1.47</b>
	Multimodal	D = 30	4.10	<b>2.61</b>	2.66	3.59	3.80	4.24
		D = 50	4.10	2.49	<b>2.42</b>	3.71	4.20	4.07
		D = 100	3.96	2.58	<b>2.14</b>	4.14	3.98	4.20
	Hybrid	D = 30	4.06	<b>2.63</b>	3.82	3.46	3.52	3.52
		D = 50	4.12	<b>2.16</b>	3.41	3.87	3.84	3.59
		D = 100	4.36	<b>1.20</b>	3.17	3.83	3.96	4.48
	Composition	D = 30	4.59	3.08	3.99	3.20	<b>2.97</b>	3.16
		D = 50	4.00	<b>3.01</b>	3.35	3.59	3.63	3.42
		D = 100	4.01	4.12	3.17	<b>3.16</b>	3.36	3.18

Bold values show the best Friedman score

benchmark suite. The F1 test function box-plot graphs (Fig. 4a–c) display that the FDBAGSK variants were superior to the base algorithm in convergence to the minimum error value in all dimensions. The results clearly show the impact of the FDB method on the exploitation ability of the FDB-based AGSK variants. The box-plots in Fig. 4d–f show that Case-1 was able to conduct a stable search in all dimensions and had an overwhelming advantage over the AGSK algorithm in convergence to the minimum error value. In the F5 multimodal problem, the AGSK suffered a premature convergence. The superior performance of Case-1 proved

that the FDB selection method had remarkably advanced the exploration ability of the AGSK. For hybrid and composition type problems, convergence to the minimum error value depends on the balanced search capability of the algorithm. The box-plots of the F18 and F21 box-plot problems indicate that the balanced search capability of the AGSK was insufficient. In contrast, the FDBAGSK variants showed a stable search performance for all dimensions.

Figure 5 shows box-plot graphs for different problem types selected from the CEC 2020 test suite to investigate the exploration, exploitation, and balanced search performance

**Table 6** Mean and standard deviation values obtained for CEC 2017 test functions

F	D	AGSK	Case-1	Case-2	Case-3	Case-4	Case-5
F1	30	2.17E + 05 (2.21E + 05)	1.37E + 05 (1.44E + 05)	<b>2.90E + 04 (3.32E + 04)</b>	6.65E + 04 (1.86E + 05)	4.22E + 04 (8.43E + 04)	7.01E + 04 (1.23E + 05)
	50	4.96E + 06 (3.57E + 06)	1.19E + 06 (9.45E + 05)	1.21E + 06 (1.73E + 06)	4.29E + 05 (4.38E + 05)	4.85E + 05 (3.99E + 05)	<b>3.73E + 05 (3.53E + 05)</b>
	100	1.29E + 08 (5.89E + 07)	3.79E + 07 (2.18E + 07)	2.58E + 07 (1.16E + 07)	1.77E + 07 (1.08E + 07)	3.17E + 07 (2.47E + 07)	<b>1.28E + 07 (1.20E + 07)</b>
F3	30	8.56E + 04 (1.92E + 04)	<b>6.72E + 04 (1.52E + 04)</b>	6.93E + 04 (1.47E + 04)	7.81E + 04 (1.62E + 04)	7.83E + 04 (1.60E + 04)	7.58E + 04 (1.93E + 04)
	50	1.86E + 05 (3.26E + 04)	<b>1.79E + 05 (2.83E + 04)</b>	1.89E + 05 (3.05E + 04)	1.89E + 05 (3.30E + 04)	1.89E + 05 (2.81E + 04)	1.84E + 05 (3.21E + 04)
F4	100	5.38E + 05 (7.17E + 04)	<b>4.93E + 05 (6.93E + 04)</b>	5.10E + 05 (7.32E + 04)	5.06E + 05 (4.99E + 04)	5.04E + 05 (5.70E + 04)	4.95E + 05 (5.90E + 04)
	30	9.50E + 01 (1.06E + 01)	<b>9.47E + 01 (8.60E + 00)</b>	1.07E + 02 (1.29E + 01)	9.87E + 01 (1.24E + 01)	1.02E + 02 (1.42E + 01)	9.82E + 01 (1.41E + 01)
	50	2.08E + 02 (2.75E + 01)	2.00E + 02 (3.54E + 01)	2.00E + 02 (3.36E + 01)	<b>1.89E + 02 (3.37E + 01)</b>	1.94E + 02 (3.77E + 01)	1.93E + 02 (3.16E + 01)
F5	100	4.17E + 02 (4.20E + 01)	<b>3.52E + 02 (5.49E + 01)</b>	4.02E + 02 (3.60E + 01)	3.79E + 02 (4.96E + 01)	3.98E + 02 (4.30E + 01)	3.65E + 02 (4.39E + 01)
	30	1.49E + 02 (1.46E + 01)	<b>1.16E + 02 (1.20E + 01)</b>	1.40E + 02 (1.39E + 01)	1.37E + 02 (1.36E + 01)	1.41E + 02 (1.61E + 01)	1.44E + 02 (1.38E + 01)
	50	3.25E + 02 (1.95E + 01)	<b>2.59E + 02 (2.01E + 01)</b>	3.04E + 02 (1.69E + 01)	3.12E + 02 (1.74E + 01)	3.14E + 02 (1.72E + 01)	3.20E + 02 (1.38E + 01)
F6	100	7.82E + 02 (2.31E + 01)	<b>6.62E + 02 (3.46E + 01)</b>	7.51E + 02 (2.20E + 01)	7.67E + 02 (3.32E + 01)	7.73E + 02 (2.53E + 01)	7.92E + 02 (2.29E + 01)
	30	1.96E + 01 (4.55E + 00)	<b>2.26E + 00 (1.34E + 00)</b>	1.53E + 01 (4.64E + 00)	1.27E + 01 (4.03E + 00)	1.50E + 01 (3.33E + 00)	1.60E + 01 (3.51E + 00)
	50	2.33E + 01 (4.66E + 00)	<b>2.54E + 00 (1.01E + 00)</b>	1.75E + 01 (4.91E + 00)	1.33E + 01 (7.00E + 00)	1.84E + 01 (5.80E + 00)	1.89E + 01 (5.21E + 00)
F7	100	2.85E + 01 (8.57E + 00)	<b>5.53E + 00 (1.69E + 00)</b>	1.57E + 01 (4.84E + 00)	1.08E + 01 (3.88E + 00)	1.67E + 01 (6.36E + 00)	1.75E + 01 (6.09E + 00)
	30	1.80E + 02 (1.50E + 01)	1.65E + 02 (2.37E + 01)	<b>1.54E + 02 (1.46E + 01)</b>	1.75E + 02 (1.21E + 01)	1.77E + 02 (1.25E + 01)	1.83E + 02 (1.14E + 01)
	50	3.61E + 02 (2.23E + 01)	3.24E + 02 (2.28E + 01)	<b>3.18E + 02 (2.44E + 01)</b>	3.64E + 02 (1.89E + 01)	3.61E + 02 (1.54E + 01)	3.72E + 02 (1.81E + 01)
F8	100	8.48E + 02 (3.37E + 01)	8.13E + 02 (2.98E + 01)	<b>7.73E + 02 (2.64E + 01)</b>	8.72E + 02 (3.15E + 01)	8.75E + 02 (2.91E + 01)	8.93E + 02 (2.96E + 01)
	30	1.59E + 02 (1.23E + 01)	<b>1.21E + 02 (1.10E + 01)</b>	1.50E + 02 (1.78E + 01)	1.47E + 02 (1.41E + 01)	1.47E + 02 (1.28E + 01)	1.51E + 02 (1.10E + 01)
	50	3.22E + 02 (2.12E + 01)	<b>2.59E + 02 (1.82E + 01)</b>	3.01E + 02 (1.82E + 01)	3.09E + 02 (1.99E + 01)	3.10E + 02 (1.81E + 01)	3.20E + 02 (1.52E + 01)
F9	100	7.78E + 02 (2.83E + 01)	<b>6.73E + 02 (3.21E + 01)</b>	7.46E + 02 (2.89E + 01)	7.69E + 02 (3.88E + 01)	7.64E + 02 (3.01E + 01)	7.87E + 02 (2.90E + 01)
	30	4.33E + 02 (2.59E + 02)	<b>8.44E + 01 (6.98E + 01)</b>	1.48E + 02 (9.81E + 01)	1.83E + 02 (1.39E + 02)	1.92E + 02 (1.48E + 02)	2.41E + 02 (1.85E + 02)
	50	8.80E + 02 (4.73E + 02)	<b>2.31E + 02 (1.72E + 02)</b>	5.97E + 02 (2.75E + 02)	3.21E + 02 (1.71E + 02)	3.97E + 02 (2.26E + 02)	3.88E + 02 (2.03E + 02)
F10	100	2.30E + 03 (6.88E + 02)	1.40E + 03 (5.72E + 02)	2.05E + 03 (6.13E + 02)	<b>1.06E + 03 (5.40E + 02)</b>	1.30E + 03 (5.74E + 02)	1.14E + 03 (4.82E + 02)
	30	5.58E + 03 (2.59E + 02)	5.57E + 03 (2.64E + 02)	5.49E + 03 (3.49E + 02)	<b>5.49E + 03 (3.02E + 02)</b>	5.57E + 03 (2.75E + 02)	5.58E + 03 (2.29E + 02)
	50	1.11E + 04 (3.79E + 02)	1.11E + 04 (3.61E + 02)	1.10E + 04 (4.25E + 02)	<b>1.10E + 04 (3.19E + 02)</b>	1.10E + 04 (4.02E + 02)	1.10E + 04 (4.57E + 02)
F11	100	2.75E + 04 (5.89E + 02)	2.74E + 04 (7.04E + 02)	2.76E + 04 (6.88E + 02)	2.75E + 04 (5.93E + 02)	2.75E + 04 (5.26E + 02)	<b>2.74E + 04 (5.34E + 02)</b>
	30	1.29E + 02 (2.93E + 01)	1.42E + 02 (4.10E + 01)	<b>1.16E + 02 (3.29E + 01)</b>	1.26E + 02 (2.60E + 01)	1.18E + 02 (2.22E + 01)	1.25E + 02 (2.38E + 01)
	50	2.50E + 02 (6.70E + 01)	2.58E + 02 (6.16E + 01)	<b>2.06E + 02 (4.10E + 01)</b>	2.44E + 02 (6.11E + 01)	2.63E + 02 (5.59E + 01)	2.55E + 02 (5.31E + 01)
F12	100	1.70E + 04 (7.59E + 03)	<b>4.80E + 03 (1.65E + 03)</b>	8.04E + 03 (2.64E + 03)	1.58E + 04 (7.36E + 03)	1.60E + 04 (7.71E + 03)	1.68E + 04 (5.88E + 03)
	30	<b>4.66E + 05 (3.64E + 05)</b>	8.17E + 05 (9.67E + 05)	4.78E + 05 (3.57E + 05)	5.50E + 05 (5.54E + 05)	5.33E + 05 (3.82E + 05)	6.88E + 05 (5.19E + 05)
	50	3.59E + 06 (1.60E + 06)	4.03E + 06 (3.37E + 06)	3.53E + 06 (1.69E + 06)	3.06E + 06 (1.66E + 06)	3.12E + 06 (1.57E + 06)	<b>2.94E + 06 (1.49E + 06)</b>
100	3.13E + 07 (1.32E + 07)	3.28E + 07 (1.85E + 07)	2.59E + 07 (8.82E + 06)	2.68E + 07 (1.19E + 07)	2.68E + 07 (1.28E + 07)	<b>2.51E + 07 (1.22E + 07)</b>	

Table 6 (continued)

F	D	AGSK	Case-1	Case-2	Case-3	Case-4	Case-5
F13	30	1.83E + 04 (1.47E + 04)	<b>1.32E + 04 (1.20E + 04)</b>	1.80E + 04 (1.03E + 04)	1.48E + 04 (1.05E + 04)	1.71E + 04 (1.09E + 04)	1.86E + 04 (1.39E + 04)
	50	2.27E + 04 (2.14E + 04)	3.70E + 04 (2.47E + 04)	<b>9.59E + 03 (5.45E + 03)</b>	2.41E + 04 (1.60E + 04)	1.93E + 04 (1.22E + 04)	2.50E + 04 (1.35E + 04)
	100	1.06E + 04 (2.98E + 03)	2.61E + 04 (1.60E + 04)	1.06E + 04 (2.32E + 03)	8.36E + 03 (3.67E + 03)	<b>6.82E + 03 (2.80E + 03)</b>	9.15E + 03 (4.45E + 03)
F14	30	1.62E + 02 (3.55E + 01)	1.54E + 02 (4.25E + 01)	1.45E + 02 (3.75E + 01)	1.45E + 02 (3.87E + 01)	1.45E + 02 (4.19E + 01)	<b>1.44E + 02 (3.16E + 01)</b>
	50	1.77E + 03 (2.20E + 03)	3.56E + 03 (6.80E + 03)	1.85E + 03 (2.16E + 03)	<b>1.41E + 03 (1.04E + 03)</b>	1.62E + 03 (2.93E + 03)	1.88E + 03 (3.20E + 03)
	100	4.36E + 05 (2.87E + 05)	<b>1.56E + 05 (1.02E + 05)</b>	2.72E + 05 (1.27E + 05)	2.93E + 05 (1.23E + 05)	3.58E + 05 (2.00E + 05)	3.07E + 05 (1.80E + 05)
F15	30	9.17E + 02 (6.29E + 02)	7.20E + 02 (7.53E + 02)	8.39E + 02 (7.16E + 02)	<b>5.01E + 02 (2.12E + 02)</b>	5.29E + 02 (2.25E + 02)	6.73E + 02 (4.64E + 02)
	50	9.35E + 03 (6.69E + 03)	1.09E + 04 (8.13E + 03)	7.68E + 03 (5.53E + 03)	6.30E + 03 (5.13E + 03)	<b>5.28E + 03 (4.44E + 03)</b>	6.02E + 03 (4.63E + 03)
	100	7.11E + 03 (4.87E + 03)	1.93E + 04 (1.17E + 04)	<b>2.65E + 03 (1.68E + 03)</b>	6.78E + 03 (6.67E + 03)	4.40E + 03 (4.81E + 03)	8.40E + 03 (5.80E + 03)
F16	30	1.16E + 03 (1.55E + 02)	<b>9.94E + 02 (1.07E + 02)</b>	1.12E + 03 (1.68E + 02)	1.09E + 03 (1.13E + 02)	1.08E + 03 (1.23E + 02)	1.12E + 03 (1.27E + 02)
	50	2.29E + 03 (1.93E + 02)	<b>1.83E + 03 (2.07E + 02)</b>	2.22E + 03 (2.24E + 02)	2.11E + 03 (1.98E + 02)	2.08E + 03 (2.07E + 02)	2.16E + 03 (1.98E + 02)
	100	6.62E + 03 (2.39E + 02)	<b>5.64E + 03 (3.57E + 02)</b>	6.50E + 03 (3.60E + 02)	6.40E + 03 (3.16E + 02)	6.35E + 03 (3.40E + 02)	6.45E + 03 (2.97E + 02)
F17	30	3.75E + 02 (8.24E + 01)	<b>3.03E + 02 (7.33E + 01)</b>	3.62E + 02 (7.02E + 01)	3.49E + 02 (6.73E + 01)	3.27E + 02 (7.54E + 01)	3.44E + 02 (7.34E + 01)
	50	1.55E + 03 (1.49E + 02)	<b>1.35E + 03 (1.67E + 02)</b>	1.48E + 03 (2.30E + 02)	1.49E + 03 (1.36E + 02)	1.44E + 03 (1.64E + 02)	1.45E + 03 (1.73E + 02)
	100	4.04E + 03 (1.92E + 02)	<b>3.56E + 03 (2.54E + 02)</b>	3.89E + 03 (2.89E + 02)	3.97E + 03 (2.53E + 02)	3.98E + 03 (2.65E + 02)	4.05E + 03 (2.06E + 02)
F18	30	9.97E + 04 (4.40E + 04)	<b>4.64E + 04 (2.92E + 04)</b>	6.45E + 04 (3.74E + 04)	6.91E + 04 (3.78E + 04)	6.79E + 04 (6.01E + 04)	7.97E + 04 (3.62E + 04)
	50	4.47E + 05 (2.97E + 05)	<b>1.27E + 05 (6.86E + 04)</b>	3.11E + 05 (3.73E + 05)	4.42E + 05 (2.85E + 05)	3.76E + 05 (2.34E + 05)	4.33E + 05 (2.24E + 05)
	100	3.41E + 06 (1.24E + 06)	<b>8.61E + 05 (3.37E + 05)</b>	2.41E + 06 (1.02E + 06)	3.19E + 06 (9.63E + 05)	3.21E + 06 (1.10E + 06)	3.18E + 06 (9.83E + 05)
F19	30	5.19E + 02 (9.81E + 02)	2.47E + 02 (2.98E + 02)	7.05E + 02 (1.63E + 03)	<b>2.40E + 02 (4.30E + 02)</b>	2.83E + 02 (5.23E + 02)	5.21E + 02 (6.43E + 02)
	50	3.39E + 03 (4.24E + 03)	<b>3.35E + 03 (4.97E + 03)</b>	6.36E + 03 (6.00E + 03)	5.49E + 03 (5.34E + 03)	6.42E + 03 (6.62E + 03)	5.57E + 03 (6.01E + 03)
	100	4.67E + 03 (4.22E + 03)	2.41E + 04 (3.08E + 04)	<b>1.90E + 03 (2.17E + 03)</b>	4.33E + 03 (5.17E + 03)	3.01E + 03 (3.49E + 03)	7.51E + 03 (1.48E + 04)
F20	30	4.65E + 02 (5.85E + 01)	<b>4.00E + 02 (7.18E + 01)</b>	4.02E + 02 (1.01E + 02)	4.38E + 02 (7.21E + 01)	4.32E + 02 (6.88E + 01)	4.40E + 02 (5.63E + 01)
	50	1.30E + 03 (1.12E + 02)	<b>1.15E + 03 (1.20E + 02)</b>	1.24E + 03 (1.89E + 02)	1.19E + 03 (1.42E + 02)	1.18E + 03 (1.28E + 02)	1.20E + 03 (1.55E + 02)
	100	4.22E + 03 (2.06E + 02)	<b>3.98E + 03 (2.23E + 02)</b>	4.09E + 03 (2.70E + 02)	4.07E + 03 (1.88E + 02)	4.08E + 03 (1.73E + 02)	4.13E + 03 (2.44E + 02)
F21	30	3.43E + 02 (1.28E + 01)	<b>3.16E + 02 (1.30E + 01)</b>	3.37E + 02 (1.29E + 01)	3.33E + 02 (1.17E + 01)	3.34E + 02 (1.49E + 01)	3.39E + 02 (1.20E + 01)
	50	5.15E + 02 (1.72E + 01)	<b>4.55E + 02 (1.33E + 01)</b>	4.97E + 02 (1.94E + 01)	4.99E + 02 (1.93E + 01)	4.97E + 02 (2.08E + 01)	5.07E + 02 (1.65E + 01)
	100	9.91E + 02 (3.04E + 01)	<b>8.98E + 02 (3.20E + 01)</b>	9.49E + 02 (2.82E + 01)	9.78E + 02 (2.72E + 01)	9.74E + 02 (2.84E + 01)	9.83E + 02 (2.92E + 01)
F22	30	2.62E + 02 (2.78E + 02)	1.58E + 02 (4.79E + 01)	2.04E + 02 (1.14E + 02)	1.36E + 02 (3.96E + 01)	1.27E + 02 (3.29E + 01)	1.66E + 02 (2.66E + 02)
	50	1.14E + 04 (1.46E + 03)	1.12E + 04 (1.70E + 03)	1.12E + 04 (1.42E + 03)	1.14E + 04 (5.43E + 02)	1.12E + 04 (1.07E + 03)	<b>1.06E + 04 (2.88E + 03)</b>
	100	<b>2.86E + 04 (5.21E + 02)</b>	2.87E + 04 (7.35E + 02)	2.87E + 04 (5.00E + 02)	2.86E + 04 (7.04E + 02)	2.86E + 04 (5.51E + 02)	2.87E + 04 (5.19E + 02)
F23	30	4.81E + 02 (1.47E + 01)	<b>4.59E + 02 (9.29E + 00)</b>	4.69E + 02 (1.31E + 01)	4.74E + 02 (8.91E + 00)	4.73E + 02 (1.16E + 01)	4.75E + 02 (1.34E + 01)
	50	7.20E + 02 (1.79E + 01)	<b>6.85E + 02 (2.47E + 01)</b>	6.94E + 02 (2.12E + 01)	7.14E + 02 (1.78E + 01)	7.16E + 02 (1.96E + 01)	7.12E + 02 (2.00E + 01)
	100	1.28E + 03 (3.27E + 01)	<b>1.21E + 03 (4.49E + 01)</b>	1.22E + 03 (3.78E + 01)	1.24E + 03 (2.51E + 01)	1.24E + 03 (2.75E + 01)	1.25E + 03 (2.56E + 01)

Table 6 (continued)

F	D	AGSK	Case-1	Case-2	Case-3	Case-4	Case-5
F24	30	5.36E + 02 (9.70E + 00)	<b>5.22E + 02 (1.17E + 01)</b>	5.30E + 02 (1.28E + 01)	5.33E + 02 (1.08E + 01)	5.29E + 02 (1.01E + 01)	5.30E + 02 (1.21E + 01)
	50	7.54E + 02 (1.56E + 01)	<b>7.37E + 02 (1.93E + 01)</b>	7.40E + 02 (1.22E + 01)	7.54E + 02 (1.86E + 01)	7.49E + 02 (1.47E + 01)	7.52E + 02 (1.58E + 01)
	100	1.54E + 03 (3.45E + 01)	1.60E + 03 (5.21E + 01)	<b>1.51E + 03 (3.56E + 01)</b>	1.55E + 03 (3.08E + 01)	1.53E + 03 (3.40E + 01)	1.54E + 03 (2.96E + 01)
F25	30	3.91E + 02 (7.66E + 009)	3.91E + 02 (6.33E + 00)	3.93E + 02 (6.00E + 00)	3.89E + 02 (4.48E + 00)	3.89E + 02 (1.52E + 00)	<b>3.89E + 02 (1.10E + 00)</b>
	50	5.71E + 02 (1.98E + 01)	<b>5.48E + 02 (1.92E + 01)</b>	5.68E + 02 (2.14E + 01)	5.64E + 02 (1.85E + 01)	5.60E + 02 (2.00E + 01)	5.59E + 02 (2.09E + 01)
F26	100	1.01E + 03 (5.70E + 01)	9.55E + 02 (5.15E + 01)	9.80E + 02 (3.96E + 01)	9.59E + 02 (5.19E + 01)	9.85E + 02 (5.64E + 01)	<b>9.37E + 02 (4.11E + 01)</b>
	30	2.30E + 03 (1.55E + 02)	<b>2.11E + 03 (2.62E + 02)</b>	2.14E + 03 (1.37E + 02)	2.13E + 03 (4.34E + 02)	2.11E + 03 (3.89E + 02)	2.13E + 03 (4.48E + 02)
	50	3.84E + 03 (1.61E + 02)	3.61E + 03 (2.03E + 02)	<b>3.58E + 03 (1.93E + 02)</b>	3.77E + 03 (1.70E + 02)	3.71E + 03 (1.75E + 02)	3.83E + 03 (1.69E + 02)
F27	100	9.89E + 03 (3.46E + 02)	1.03E + 04 (4.61E + 02)	<b>9.35E + 03 (3.63E + 02)</b>	9.78E + 03 (2.90E + 02)	9.70E + 03 (2.44E + 02)	9.86E + 03 (3.04E + 02)
	30	<b>5.22E + 02 (1.24E + 01)</b>	5.24E + 02 (1.48E + 01)	5.30E + 02 (1.81E + 01)	5.22E + 02 (9.92E + 00)	5.25E + 02 (1.53E + 01)	5.24E + 02 (9.49E + 00)
	50	7.30E + 02 (1.01E + 02)	6.51E + 02 (8.64E + 01)	7.66E + 02 (1.15E + 02)	<b>6.60E + 02 (7.86E + 01)</b>	7.00E + 02 (9.00E + 01)	7.05E + 02 (9.90E + 01)
F28	100	7.64E + 02 (3.08E + 01)	7.55E + 02 (4.12E + 01)	8.22E + 02 (3.62E + 01)	7.43E + 02 (2.86E + 01)	7.44E + 02 (2.98E + 01)	<b>7.35E + 02 (2.70E + 01)</b>
	30	4.47E + 02 (1.72E + 01)	4.50E + 02 (2.42E + 01)	4.41E + 02 (2.04E + 01)	4.40E + 02 (1.76E + 01)	4.39E + 02 (1.88E + 01)	<b>4.35E + 02 (1.57E + 01)</b>
F29	50	5.35E + 02 (3.07E + 01)	5.34E + 02 (3.02E + 01)	5.60E + 02 (2.71E + 01)	5.25E + 02 (2.88E + 01)	5.32E + 02 (3.07E + 01)	<b>5.22E + 02 (2.77E + 01)</b>
	10	<b>8.35E + 02 (5.83E + 01)</b>	8.52E + 02 (2.20E + 02)	8.39E + 02 (5.86E + 01)	7.96E + 02 (5.31E + 01)	8.45E + 02 (5.95E + 01)	7.66E + 02 (5.21E + 01)
	30	1.04E + 03 (1.18E + 02)	<b>8.94E + 02 (1.08E + 02)</b>	9.78E + 02 (1.15E + 02)	1.01E + 03 (1.10E + 02)	9.82E + 02 (8.28E + 01)	9.93E + 02 (8.11E + 01)
F30	50	1.68E + 03 (1.68E + 02)	1.48E + 03 (2.43E + 02)	1.68E + 03 (1.78E + 02)	1.66E + 03 (1.86E + 029)	1.69E + 03 (1.74E + 02)	1.74E + 03 (1.56E + 02)
	100	5.18E + 03 (2.64E + 02)	<b>4.66E + 03 (4.15E + 02)</b>	5.02E + 03 (3.48E + 02)	5.07E + 03 (3.11E + 02)	5.05E + 03 (3.78E + 02)	5.11E + 03 (3.39E + 02)
	30	1.21E + 04 (6.58E + 03)	1.42E + 04 (7.43E + 03)	<b>1.12E + 04 (4.71E + 03)</b>	1.31E + 04 (5.58E + 03)	1.47E + 04 (8.12E + 03)	1.56E + 04 (8.24E + 03)
F30	50	1.31E + 06 (3.53E + 05)	1.38E + 06 (3.50E + 05)	<b>1.24E + 06 (2.45E + 05)</b>	1.27E + 06 (2.78E + 05)	1.39E + 06 (2.63E + 05)	1.37E + 06 (3.72E + 05)
	100	7.22E + 04 (3.71E + 04)	1.07E + 05 (6.53E + 04)	9.57E + 04 (4.00E + 04)	4.22E + 04 (1.98E + 04)	<b>4.20E + 04 (2.05E + 04)</b>	5.07E + 04 (3.31E + 04)

Bold values indicate the best mean and standard deviation results

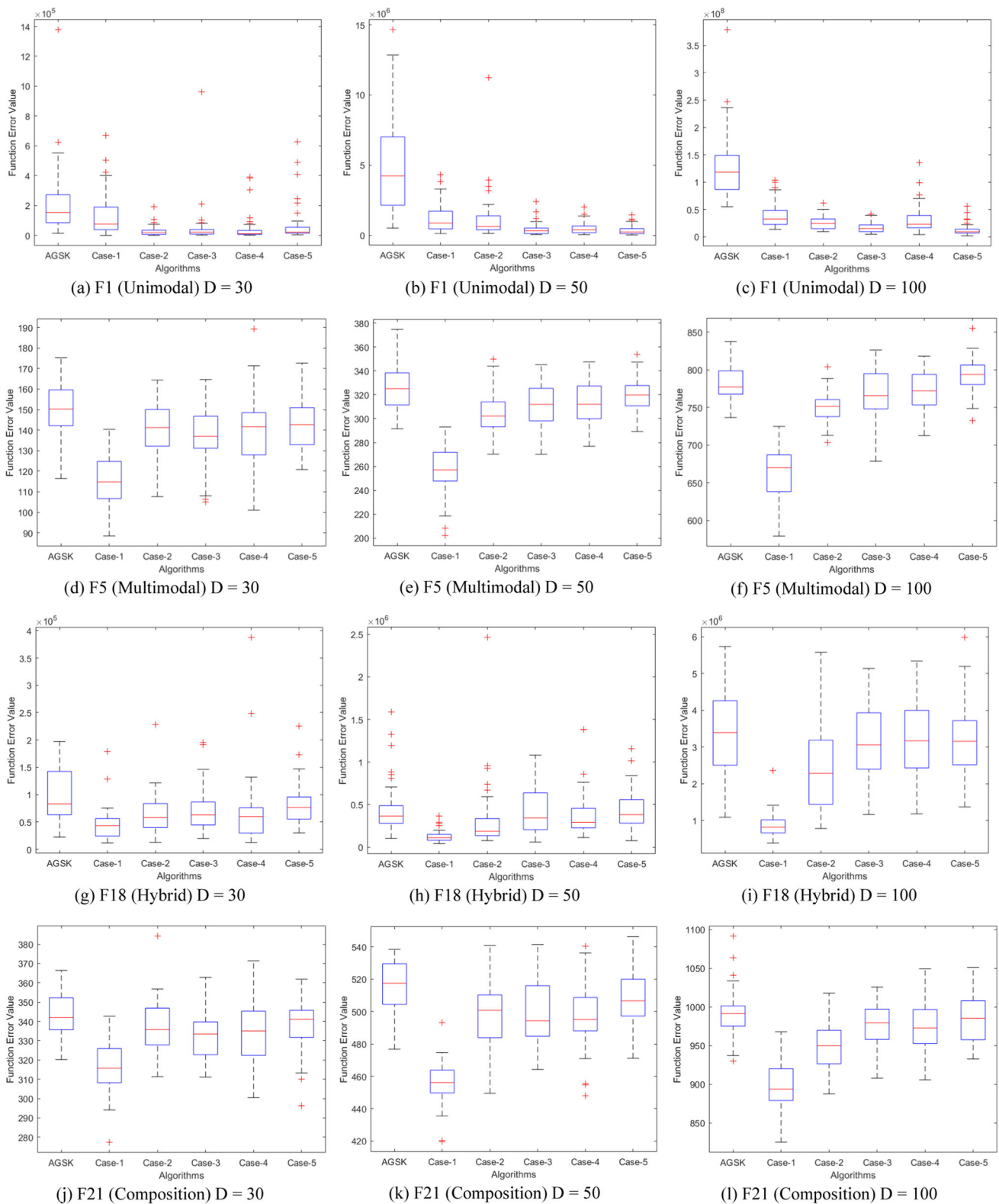
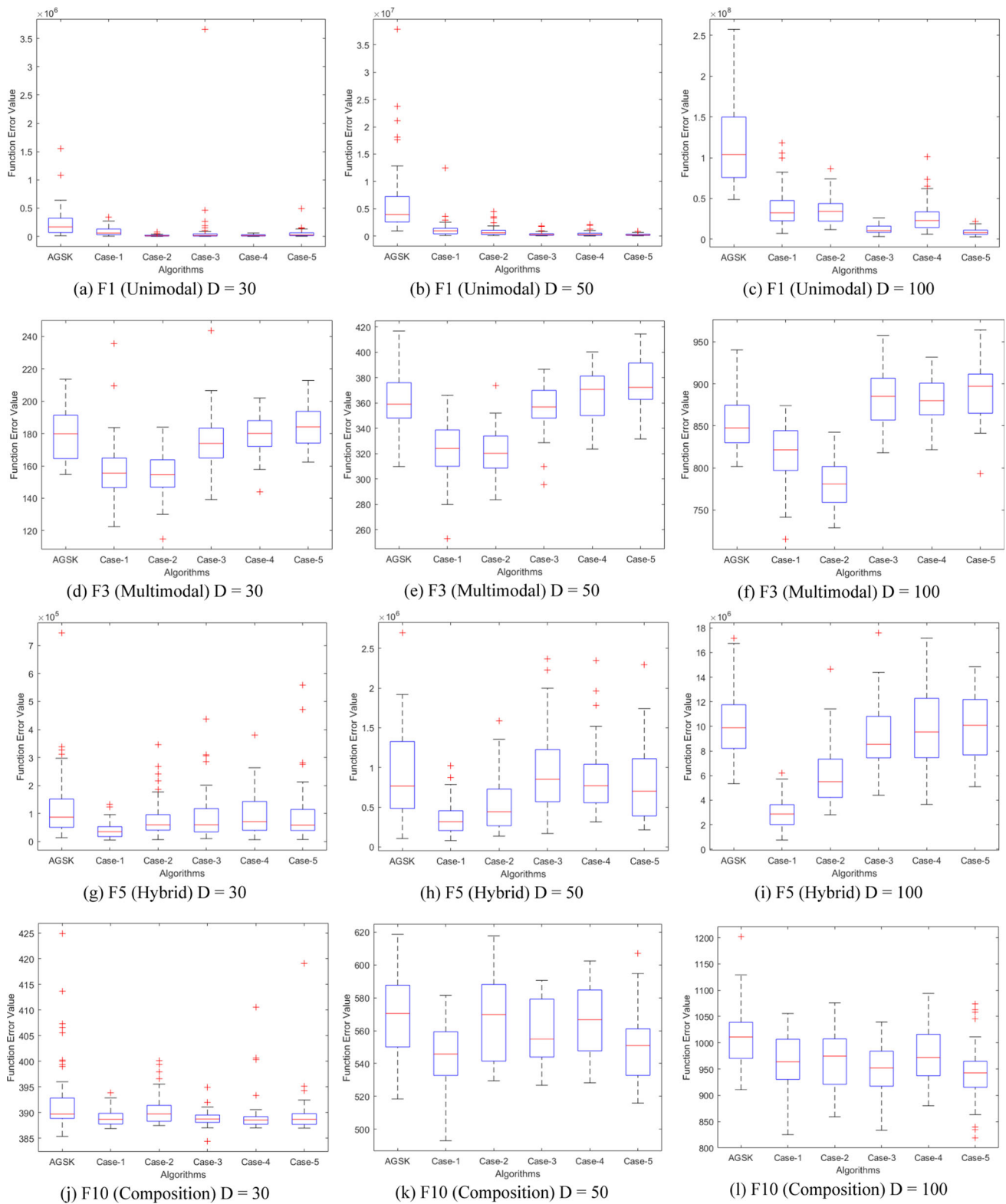


Fig. 4 Box-plot graphs for unimodal, multimodal, hybrid, and composition benchmark functions of the CEC 2017 test suite



**Fig. 5** Box-plot graphs for unimodal, multimodal, hybrid, and composition benchmark functions of the CEC 2020 test suite

of the AGSK and the FDBAGSK variants. The exploitation capability of the FDBAGSK variants in the unimodal (F1) problem type, designed to test the exploitation ability of algorithms, was superior to that of the base algorithm. Solving the multimodal (F3) problem including many local solution traps requires a strong exploration ability. Accordingly, Case-1 and Case-2 variants managed to converge to the minimum error value in all dimensions with their powerful exploration capability. In hybrid (F8) and composition (F10) problem types, the convergence rate depends on the algorithm successfully balancing exploration and exploitation. The graphs in Fig. 5g–l display that the balanced search ability of the FDB-based Case-1 variant was stronger than that of its competitors.

### 5.1.2 Convergence analysis

In this section, the convergence performance of the AGSK and FDBAGSK variants is examined. The convergence ability of the algorithms was evaluated on the unimodal (F1), multimodal (F9), hybrid (F16), and composition (F29) type test functions of the CEC 2017 benchmark suite. Figure 6 shows the convergence curves of the algorithms for the different problem types in 30, 50, and 100 dimensions.

The unimodal F1 function curves in Fig. 6a–c demonstrate that the algorithms were successful in solving the unimodal problem type designed to investigate the exploitation ability. The FDBAGSK variants were superior to the AGSK in fulfilling the task of exploitation. Because the multimodal F9 problem contains many local solution traps, an algorithm must have a powerful exploration ability in order to solve this problem. The convergence curves in Fig. 6d–f show that the AGSK algorithm gets stuck in the local optimum and therefore had a premature convergence problem. When the convergence curves for the F9 multimodal problem were analyzed in depth, it was observed that the FDBAGSK variants outperformed AGSK in terms of solution accuracy. This can be explained by the fact that the FDB selection method improves the exploration capability of the AGSK algorithm. Effective exploration of the search spaces in hybrid and composition type problems depends on the powerful exploration–exploitation balance. The convergence curves in Fig. 6g–l depict that the AGSK method had difficulty in achieving the exploration–exploitation balance. On the other hand, the FDB-based AGSK variants outperformed the base AGSK algorithm in optimizing F16 hybrid and F29 composition problems for 30, 50, and 100 dimensions.

As a result, the convergence graphs in Fig. 6 illustrate that the AGSK algorithm was deficient in fulfilling the exploration and exploitation tasks. The AGSK could not converge to a global optimum due to the premature convergence problem. On the other hand, the convergence performance of the FDBAGSK variants was remarkable. The FDB-based AGSK

variants outperformed the base algorithm in different search spaces and challenging benchmark problems. The underlying reason for the superiority of the FDBAGSK variants was the efficient design of the selection phase of the AGSK algorithm with the FDB method, thereby empowering exploration and exploitation operators.

### 5.1.3 Algorithm complexity

Algorithm complexity provides researchers with information about the usability and functionality of an algorithm. This subcategory presents the algorithm complexity knowledge of the FDBAGSK variants. The IEEE CEC 2014 definition document [46] was referenced to calculate algorithm complexity. Accordingly, the three parameters  $T_0$ ,  $T_1$ , and  $T_2$  were used in the algorithm complexity calculation.  $T_0$  corresponds to the calculation time of the algorithm for a test program defined in CEC 2014.  $T_1$  signifies the time taken for the algorithm to calculate the F18 test problem once, as one of the CEC 2014 benchmark problems.  $T_2$  represents the mean time taken to calculate the same test problem five times. In light of these definitions, the algorithm complexity was calculated using the  $(T_2 - T_1)/T_0$  formula.

The algorithm complexity of the AGSK and FDBAGSK variants (Case-1, ..., Case-5) on 30/50/100 dimensions are presented in Table 7. As it can be seen from the table, the algorithm complexity of the AGSK and the FDBAGSK variants is very close in all dimensions. The stable performance of the FDBAGSK versions in terms of algorithm complexity, despite the increase in search space dimensions, is an indication that they could be powerful alternatives for high-dimensional optimization problems. In addition, although the FDB selection method added extra computational procedures in the search-process lifecycle, the fact that the algorithm complexity of the FDBAGSK variants had only slightly increased compared to the base algorithm was impressive.

Figure 7 visualizes the numerical results given in Table 7. It is clear from the figure that the FDB selection method had only slightly increased the algorithm complexity. In general, algorithm complexity was low for all algorithms. The algorithm complexity for both the AGSK and FDBAGSK variants was slightly affected by search space dimension changes.

The experimental studies in Sect. 5.1 investigated the influence of the FDB selection method on the AGSK search performance for different problem types in the CEC 2017 and CEC 2020 benchmark test suites. The results showed that the FDB-based AGSK variants were able to eliminate the premature convergence problem and yielded a better search performance compared to the AGSK algorithm. In addition, when the FDBAGSK variants were evaluated among themselves, Case-1 was determined as the most successful variant.

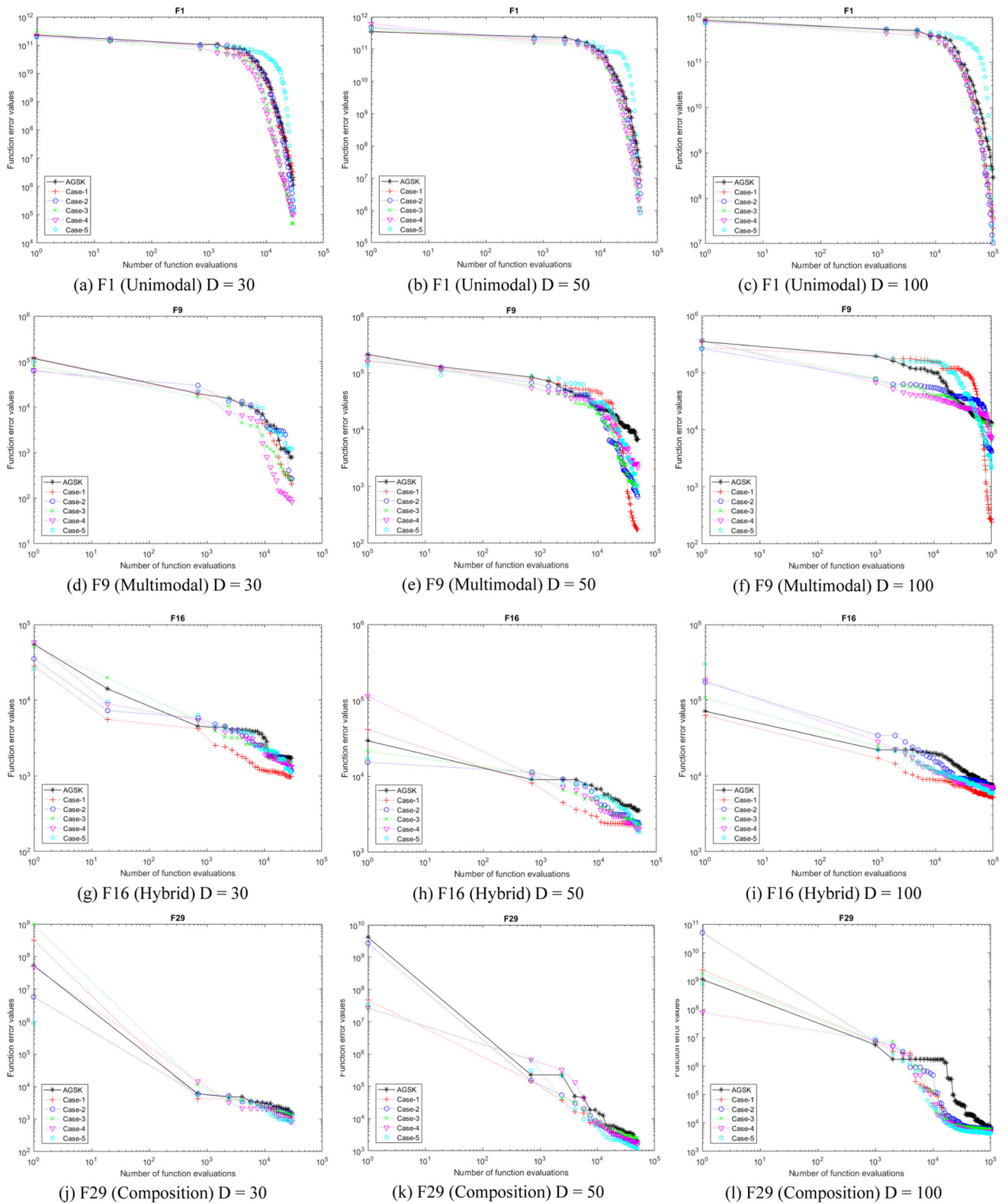


**Fig. 6** Convergence curves of AGSK and FDBAGSK variants for the CEC 2017 benchmark suite unimodal, multimodal, hybrid, and composition function types

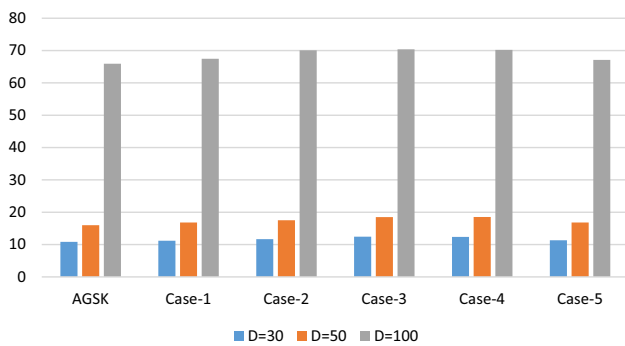


Fig. 7 Algorithm complexity for AGSK and FDBAGSK variants

Case-1 will be referred to as FDBAGSK in the following sections. The next sub-section is concerned with optimizing the ORPF problem.

### 5.2 Application of the proposed FDBAGSK algorithm to the solution of the AC/DC-ORPF problem

In this sub-section, the proposed FDBAGSK and AGSK algorithms were applied to solve the AC/DC-ORPF problem incorporating multi-DGs and HVDC systems. Power flow calculations were performed via MATPOWER 6.0. [47]. As a rule of thumb, the maximum number of iterations and population size were accepted as 200 and 30, respectively. Algorithms were run 20 times for each simulation case and the best, worst, mean, and standard deviation values were recorded.

Table 8 presents a summary of the IEEE 30- and 57-bus test system configurations including the bus, branch, generator, transformer, and shunt capacitor. The total active and reactive power load demands of the IEEE 30- bus test system were 2.834 and 1.262 p.u. at the 100 MVA base, respectively. The total active and reactive power load demands of the IEEE 57- bus test system were 12.508 and 3.364 p.u. at the 100 MVA base, respectively. Table 9 gives the limit values of the state variables for the AC/DC-ORPF problem and Table 10 presents the minimum and maximum limits of the AC and DC control variables. The schematic diagram given in Fig. 8 illustrates the implementation steps of the proposed FDBAGSK method for the AC/DC-ORPF problem.

The effectiveness of the proposed FDBAGSK method has been evaluated on modified IEEE 30- and 57-bus power systems incorporating DGs and HVDC systems. In this regard, twelve different test cases were optimized given in Table 11.

#### 5.2.1 Modified IEEE-30 bus test system

In this subcategory, seven test cases are studied to solve the ORPF problem in the modified IEEE 30-bus test system with DGs and HVDC transmission links.

**Case-1: Minimization of active power loss with HVDC at (2–14)** In Case-1, the active power loss minimization has been studied with two-terminal HVDC located between buses 2 and 14 of the modified IEEE 30-bus test system. Table 12 gives the simulation results of FDBAGSK and AGSK algorithms. Accordingly, the power loss values obtained from the proposed FDBAGSK and AGSK algorithms are **11.4208 MW** and 11.5165 MW respectively. The objective function value of the proposed algorithm is **0.8379%** lower than that of the AGSK. Figure 9a depicts the variation of power loss with respect to the number of iterations for regarding test case. As can be seen from the figure, FDBAGSK successfully performed the exploitation task in the last stages of the optimization process and achieved a better value compared to AGSK. Figure 9b demonstrates that the load bus voltages obtained by all optimization algorithms were within acceptable limits (0.95–1.05 p.u).

**Case-2: Minimization of active power loss with HVDC at (2–16)** Case-2 optimizes the active power loss of the IEEE 30-bus test system modified with a two-terminal HVDC between buses 2 and 16. The simulation results of Case-2 are reported in Table 12. From the numerical results, it is observed that the proposed method was more successful in minimizing active power loss compared to the AGSK. To put it more clearly, the proposed FDBAGSK offered the minimum power loss value of **11.0921 MW**, which is lower by **0.2248%** than the AGSK simulation result. An in-depth analysis of the convergence curves given in Fig. 10a gave that although for Case-2 the algorithms yielded similar performances in terms of convergence speed, the proposed method was superior to the AGSK in terms of convergence accuracy. The graph given in Fig. 10b was drawn to visualize the voltage profile of the load buses for the present case. The relevant

Table 7 Algorithm complexity

Dimension	T0	T1	AGSK	Case-1	Case-2	Case-3	Case-4	Case-5
$D = 30$	0.0835	0.7196	10.8256	11.2007	11.6684	12.4257	12.3683	11.3258
$D = 50$		1.2782	15.9880	16.8325	17.5389	18.4981	18.5160	16.8157
$D = 100$		3.9926	65.9463	67.4490	70.0552	70.4011	70.1947	67.1269

**Table 8** Configuration of the test systems

Characteristics	IEEE 30-bus test system		IEEE 57-bus test system	
	Number	Details	Number	Details
Buses	30	[48]	57	[49]
Branches	41	[48]	80	[49]
Thermal generators	5	Buses: 2, 5, 8, 11 and 13	6	Buses: 2, 3,6, 8, 9 and 12
Swing generator	1	Buses:1	1	Buses:1
Transformers	4	Branches: 11, 12, 15 and 36	17	Branches:19, 20, 31, 35, 36, 37, 41, 46, 54, 58, 59, 65, 66, 71, 73, 76 and 80
Shunt capacitors	2	Buses: 10 and 24	3	Buses: 18, 25 and 53

**Table 9** Minimum and maximum limits of state variables [14]

Variables ( $M^{AC}$ )	$M^{AC}_{min}$	$M^{AC}_{max}$	Variables ( $M^{DC}$ )	$M^{DC}_{min}$	$M^{DC}_{max}$
<i>IEEE 30- bus test system</i>					
$P_{THG_1}$ (MW)	0	360.2	$t_r$	0.90	1.10
$Q_{THG_1}$ (MVar)	− 100	100	$t_i$	0.90	1.10
$Q_{THG_2}$ (MVar)	− 40	50			
$Q_{THG_5}$ (MVar)	− 40	40	$\alpha_r$ (°)	9.74	22.91
$Q_{THG_8}$ (MVar)	− 10	40			
$Q_{THG_{11}}$ (MVar)	− 6	24			
$Q_{THG_{13}}$ (MVar)	− 6	24	$\gamma_i$ (°)	8.59	22.91
$V_{L_1} \dots V_{L_{NPQ}}$ (p.u.)	0.95	1.05	$v_{dr}$ (p.u.)	1.00	1.50
			$v_{di}$ (p.u.)	1.00	1.50
<i>IEEE 57-bus test system</i>					
$P_{THG_1}$ (MW)	20	50	$t_r$	0.90	1.10
$Q_{THG_1}$ (MVar)	− 100	100	$t_i$	0.90	1.10
$Q_{THG_2}$ (MVar)	− 17	50			
$Q_{THG_3}$ (MVar)	− 10	60	$\alpha_r$ (°)	5.00	30.00
$Q_{THG_6}$ (MVar)	− 8	25			
$Q_{THG_8}$ (MVar)	− 140	200			
$Q_{THG_9}$ (MVar)	− 3	9	$\gamma_i$ (°)	10.00	30.00
$Q_{THG_{12}}$ (MVar)	− 150	155	$v_{dr}$ (p.u.)	1.00	1.40
$V_{L_1} \dots V_{L_{NPQ}}$ (p.u.)	0.94	1.06	$v_{di}$ (p.u.)	1.00	1.40

figure showed that all algorithms are successful in keeping the load bus voltages within acceptable limits.

**Case-3: Minimization of active power loss with 3-DGs** In this case, minimization of active power loss in an IEEE 30-bus power system including three DG units are studied. Additionally, the allocations, i.e., both the location and sizing of the DG units are optimized. According to the comparative simulation results given in Table 12, the objective function values obtained by the FDBAGSK and AGSK methods are **9.2984 MW** and **9.3182 MW**, respectively. The simulation results indicated that the proposed FDBAGSK provided a **0.2124%** decrease in active power loss compared to the AGSK. Figure 11a illustrates the convergence curves of the

FDBAGSK and AGSK algorithms for Case-3. As it can be seen from the figure, FDBAGSK exhibited a robust and stable search performance. The voltage profile given in Fig. 11b shows that the voltage constraint is satisfied for all load buses.

**Case-4: Minimization of active power loss with both 3-DGs and HVDC at (2–14)** The optimization algorithms have been run minimization of active power loss in a modified IEEE 30-bus test system incorporating HVDC systems and DG units. The obtained solutions are given in Table 12. From the numeric results, it can be seen that FDBAGSK achieved a lower power loss **8.7366 MW** than AGSK (8.8093 MW). Quantitatively, the proposed algorithm provided a **0.8252%** reduction in the objective function value. It is evident that

**Table 10** Minimum and maximum limits of control variables [14]

Variables ( $P^{AC}$ )	$P_{min}^{AC}$	$P_{max}^{AC}$	Variables ( $P^{DC}$ )	$P_{min}^{DC}$	$P_{max}^{DC}$
<i>IEEE 30-bus test system</i>					
$P_{THG_2}$ (MW)	0	140	$P_r$ (p.u.)	0.1	1.50
$V_{THG_1}$ (p.u.)	1.00	1.15			
$V_{THG_2}$ (p.u.)	1.00	1.15	$P_i$ (p.u.)	0.1	1.50
$V_{THG_5}$ (p.u.)	1.00	1.15			
$V_{THG_8}$ (p.u.)	1.00	1.15	$Q_r$ (p.u.)	0.001	0.75
$V_{THG_{11}}$ (p.u.)	1.00	1.15			
$V_{THG_{13}}$ (p.u.)	1.00	1.15	$Q_i$ (p.u.)	0.001	0.75
$T_1 \dots T_{NT}$ (p.u.)	0.90	1.10	$i_d$	0.1	1.00
$P_{DG1} \dots P_{DGN DG}$ (MW)	0	10			
$loc_{DG1} \dots loc_{DGN DG}$	1	29			
<i>IEEE 57-bus test system</i>					
Variables ( $P^{AC}$ )	$P_{min}^{AC}$	$P_{max}^{AC}$	Variables ( $P^{DC}$ )	$P_{min}^{DC}$	$P_{max}^{DC}$
$P_{THG_2}$ (MW)	15	90	$P_r$ (p.u.)	0.1	1.50
$P_{THG_3}$ (MW)	10	500			
$P_{THG_6}$ (MW)	10	50	$P_i$ (p.u.)	0.1	1.50
$P_{THG_8}$ (MW)	12	50			
$P_{THG_9}$ (MW)	10	360	$Q_r$ (p.u.)	0.001	0.75
$P_{THG_{12}}$ (MW)	5	550			
$V_{THG_1}$ (p.u.)	0.9	1.1	$Q_i$ (p.u.)	0.001	0.75
$V_{THG_2}$ (p.u.)	0.9	1.1			
$V_{THG_3}$ (p.u.)	0.9	1.1	$i_d$	0.05	1.00
$V_{THG_6}$ (p.u.)	0.9	1.1			
$V_{THG_8}$ (p.u.)	0.9	1.1			
$V_{THG_9}$ (p.u.)	0.9	1.1			
$V_{THG_{12}}$ (p.u.)	0.9	1.1			
$T_1 \dots T_{NT}$ (p.u.)	0.9	1.1			
$P_{DG1} \dots P_{DGN DG}$ (MW)	0	30			
$loc_{DG1} \dots loc_{DGN DG}$	1	56			

the proposed FDBAGSK is very effective in optimizing the system. Figure 12a and b illustrates the convergence curves of the optimization algorithms for Case-4 and the voltage profile of the load buses obtained as a result of the simulation, respectively. The convergence curves show that the proposed FDBAGSK exhibited a better search performance than the AGSK in terms of convergence speed and accuracy. In addition, Fig. 12b demonstrates that the voltage values of the load buses were within the specified limits.

**Case-5: Minimization of active power loss with both 3-DGs and HVDC at (2–16)** This case optimizes the active power loss in the IEEE 30-bus power system inclusion of DGs and HVDC. The size and location of DGs are considered as control variables. HVDC is integrated between buses 2 and 16 of the power system. The FDBAGSK and AGSK algorithms are applied to obtain the ORPF solutions, and the results are

presented in Table 12. The simulation result obtained from the proposed algorithm is **8.2344 MW**, which was **0.0570%** lower than the result of the AGSK algorithm. Figure 13a shows the fitness value obtained by the algorithms depending on the number of iterations. The relevant figure shows that the proposed algorithm reaches the best value faster than the original AGSK algorithm. The voltage profile graph given in Fig. 13b confirms that the voltage value of the load buses is within the specified limits.

**Case-6: Minimization of voltage deviation with both 3-DGs and HVDC at (2–16)** In Case-6, the ORPF control variables are optimized considering the voltage deviation objective function. The present test case also handles the optimal placement of DGs. The HVDC is located between buses 2 and 16 of the IEEE-30 bus test system. From Table 12, it is seen that the voltage deviation value obtained by FDBAGSK is

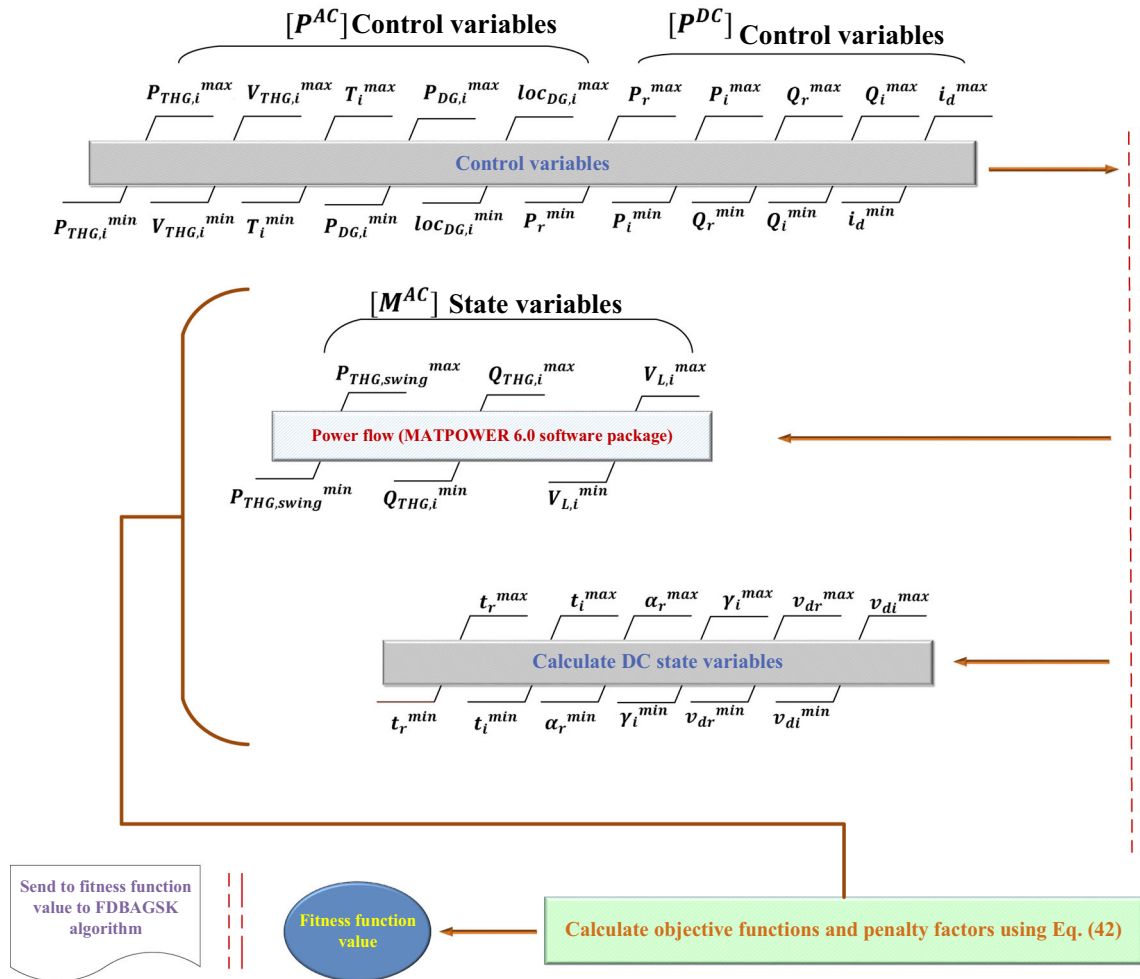


Fig. 8 AC/DC-ORPF problem optimization process

Table 11 Simulation test cases

Study cases	IEEE 30-bus test system					
	$P_{loss}$	$VD$	$L - index$	3-DGs	HVDC at (2–14)	HVDC at (2–16)
Case-1	✓	–	–	–	✓	–
Case-2	✓	–	–	–	–	✓
Case-3	✓	–	–	✓	–	–
Case-4	✓	–	–	✓	✓	–
Case-5	✓	–	–	✓	–	✓
Case-6	–	✓	–	✓	–	✓
Case-7	–	–	✓	✓	–	✓
Study cases	IEEE 57-bus test system					
	$P_{loss}$	$VD$	$L - index$	3-DGs	HVDC at (8–9)	
Case-8	✓	–	–	–	✓	
Case-9	✓	–	–	✓	–	
Case-10	✓	–	–	✓	✓	
Case-11	–	✓	–	✓	✓	
Case-12	–	–	✓	✓	✓	

**Table 12** Simulation results for the IEEE 30-bus test system

Parameters	Case-1		Case-2		Case-3		Case-4		Case-5		Case-6		Case-7	
	AGSK	FDBAGSK												
$P_{THG1}$	155.1764	154.8529	154.5713	154.5138	122.9623	122.7181	133.1428	122.3779	121.6531	121.6550	162.4578	167.3362	139.9377	145.4780
$P_{THG2}$	139.7581	139.9792	139.9596	139.9906	139.9846	139.9919	139.9146	139.9413	140	139.9952	111.0879	106.9425	132.0091	126.9718
$Q_{THG1}$	-4.8523	-1.52039	3.42176	-3.8792	-3.3560	-8.5582	-3.7745	9.8478	-5.4042	-2.3202	1.1118	20.2677	47.0746	99.7263
$Q_{THG2}$	30.5790	30.8157	30.7258	40.5468	23.1243	22.7326	30.7094	30.2389	31.0039	31.5211	35.0257	39.6685	12.3071	-5.1872
$Q_{THG5}$	32.2826	35.0480	32.2685	31.7673	30.8555	28.8578	31.4810	25.1780	29.6142	29.3328	39.0287	34.7530	13.5131	-8.9432
$Q_{THG8}$	37.1424	29.6735	34.6844	28.0358	32.0068	29.9490	26.9206	35.0002	30.4424	28.8048	39.5134	16.2684	32.8524	16.5622
$Q_{THG11}$	22.2749	11.1531	4.59555	23.4450	20.8151	22.3768	21.3298	5.1876	14.0537	19.8629	17.5664	18.3119	-4.6946	21.0597
$Q_{THG13}$	10.2787	17.1492	13.8808	9.0022	4.2341	12.3223	9.1224	7.8357	13.8104	9.1559	8.5202	1.6832	21.0203	2.1795
$V_{THG1}$	1.0796	1.0829	1.0852	1.0831	1.0806	1.0765	1.0782	1.0840	1.0752	1.0770	1.0453	1.0647	1.0634	1.1160
$V_{THG2}$	1.0668	1.0695	1.0700	1.0711	1.0719	1.0693	1.0675	1.0694	1.0656	1.0663	1.0290	1.0420	1.0301	1.0631
$V_{THG5}$	1.0332	1.0351	1.0322	1.0337	1.0360	1.0324	1.0319	1.0277	1.0309	1.0313	0.9998	1.0016	0.9694	0.9791
$V_{THG8}$	1.0395	1.0323	1.0336	1.0337	1.0379	1.0366	1.0344	1.0363	1.0368	1.0367	1.0010	0.9910	0.9892	1.0129
$V_{THG11}$	1.0748	1.0687	1.0567	1.0860	1.0648	1.0748	1.0805	1.0440	1.0693	1.0781	1.0357	1.0465	0.9957	1.0841
$V_{THG13}$	1.0417	1.0666	1.0671	1.0615	1.0482	1.0661	1.0388	1.0590	1.0681	1.0620	1.0276	1.0161	1.0409	1.0515
$T_{11}$	1.0118	0.9747	0.9919	1.0523	1.0877	1.0839	0.9993	1.0113	1.0375	1.0559	1.0592	1.0266	0.9809	1.0253
$T_{12}$	1.0992	1.0884	0.9513	0.9239	0.9123	0.9019	1.0940	0.9992	0.9201	0.9139	0.9003	0.9415	0.9353	0.9113
$T_{15}$	0.9813	0.9840	0.9760	0.9656	0.9687	0.9816	0.9858	0.9531	0.9795	0.9697	0.9433	0.9435	0.9904	0.9459
$T_{36}$	0.9900	0.9527	0.9872	0.9554	0.9696	0.9605	0.9781	0.9706	0.9665	0.9646	0.9390	0.9368	0.9141	0.9478
$P_r$	0.3144	0.2588	0.2724	0.2690	-	-	0.2474	0.2620	0.2958	0.2905	0.3063	0.2678	0.2948	0.2625

Table 12 (continued)

Parameters	Case-1		Case-2		Case-3		Case-4		Case-5		Case-6		Case-7	
	AGSK	FDBAGSK	AGSK	FDBAGSK	AGSK	FDBAGSK	AGSK	FDBAGSK	AGSK	FDBAGSK	AGSK	FDBAGSK	AGSK	FDBAGSK
$P_i$	0.3142	0.2587	0.2723	0.2689	-	-	0.2473	0.2619	0.2957	0.2904	0.3061	0.2676	0.2946	0.2624
$Q_r$	0.1094	0.0741	0.0703	0.1154	-	-	0.0772	0.0962	0.1083	0.1234	0.1359	0.0954	0.0813	0.1007
$Q_i$	0.0633	0.0485	0.0543	0.0712	-	-	0.0502	0.0619	0.0545	0.0537	0.1346	0.0991	0.0589	0.0595
$t_r$	0.9960	1.0141	0.9606	1.0560	-	-	0.9359	1.0324	1.0986	1.0994	1.0311	0.9885	0.9129	1.0709
$t_i$	0.9921	1.0147	0.9702	1.0291	-	-	0.9470	1.0149	1.0654	1.0462	1.0543	1.0291	0.9155	1.0419
$\alpha_r(^{\circ})$	17.1191	14.0506	11.9153	21.9110	-	-	15.3085	18.6686	18.5910	21.6996	22.2684	17.7794	12.2556	19.6266
$\gamma(^{\circ})$	9.2258	8.8751	9.3804	13.6003	-	-	9.6404	11.9340	8.6066	8.6152	22.7872	19.3298	8.7725	11.4145
$v_{dr}$	1.3551	1.4081	1.3442	1.4038	-	-	1.2880	1.3995	1.4845	1.4572	1.3098	1.3104	1.2244	1.4355
$v_{di}$	1.3544	1.4075	1.3435	1.4032	-	-	1.2874	1.3989	1.4839	1.4566	1.3090	1.3097	1.2236	1.4349
$i_d$	0.2320	0.1838	0.2027	0.1916	-	-	0.1921	0.1872	0.1993	0.1994	0.2338	0.2044	0.2408	0.1828
$P_{DC1}(loc_{DC1})$	-	-	-	-	9.9958	9.9921	9.9747(29)	9.9722	10 (7)	9.9999	1.4569(19)	8.4629	9.9159(29)	9.9992 (24)
$P_{DC2}(loc_{DC2})$	-	-	-	-	(7)	(19)	9.9877(29)	9.9103	10 (29)	9.9996	9.8340	2.1937	9.8752(25)	9.9775 (29)
$P_{DC3}(loc_{DC3})$	-	-	-	-	9.9417(19)	9.9963	9.9396(21)	9.9466	9.9993(24)	9.9999(29)	9.8045	9.6879(20)	2.2126(19)	2.3082 (3)
$P_{loss}(MW)$	11.5165	<b>11.4208</b>	11.1171	<b>11.0921</b>	9.3182	<b>9.2984</b>	8.8093	<b>8.7366</b>	8.2391	<b>8.2344</b>	11.2229	11.2093	10.5313	11.3236
$VD(p.u.)$	0.4033	0.6508	0.7182	0.8396	0.7320	0.8900	0.5053	0.6771	0.9253	0.9246	0.1548	<b>0.1539</b>	0.2939	0.8332
$L - index$	0.1419	0.1354	0.1390	0.1339	0.1276	0.1254	0.0840	0.1309	0.0815	0.0894	0.1386	0.1327	0.0854	<b>0.0832</b>

Bold values show the best objective function value

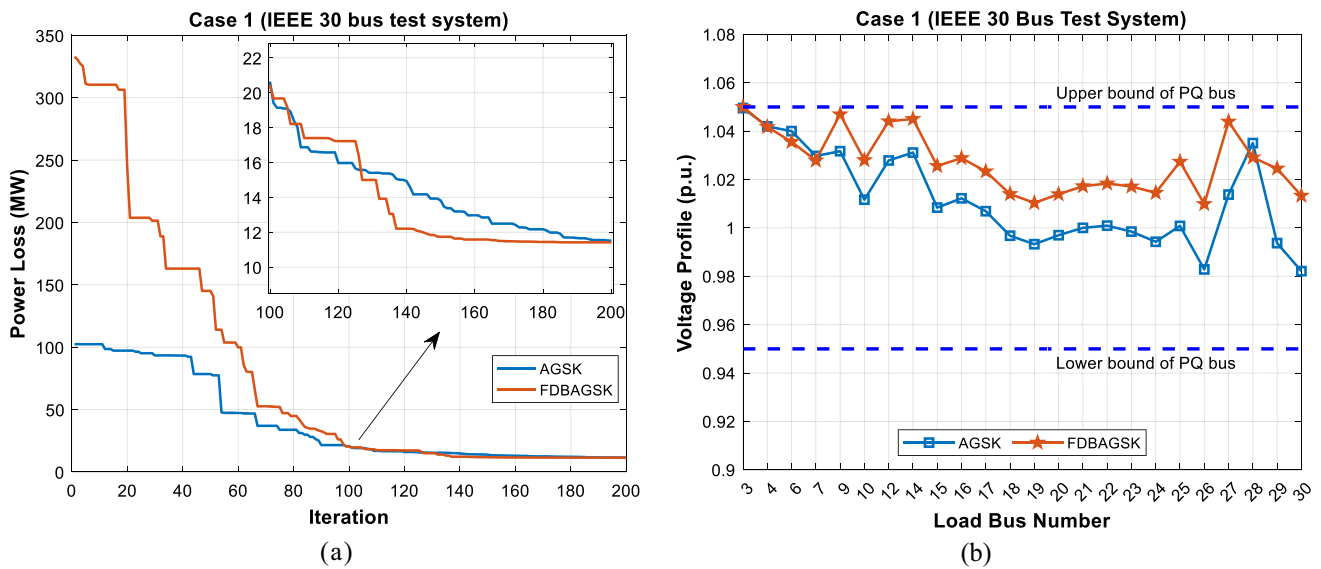


Fig. 9 Case-1: **a** Convergence curve of optimization algorithms, **b** Voltage profile of load buses

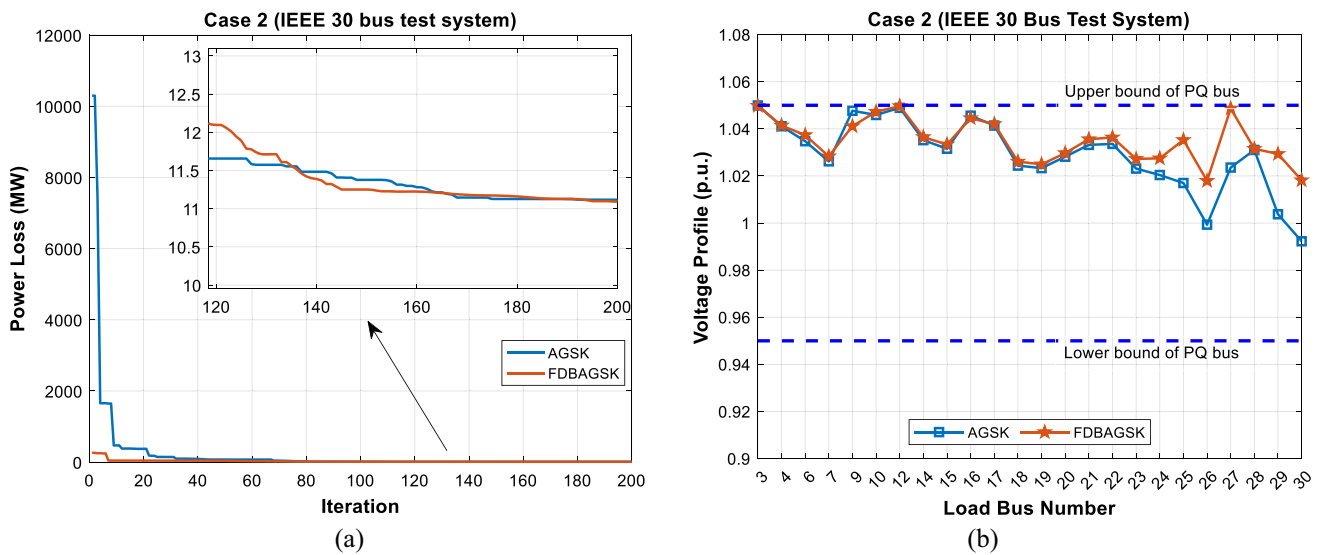


Fig. 10 Case-2: **a** Convergence curve of optimization algorithms, **b** voltage profile of load buses

**0.1539 p.u.** The objective function value is **0.5814%** lower compared to the AGSK simulation result. The optimization results demonstrate the superiority of FDBAGSK compared to the original AGSK in terms of solution quality. The convergence performance of the algorithms is illustrated in Fig. 14a. As can be seen from the figure, the proposed algorithm has lower objective function values than AGSK at the beginning of the optimization process. Although the algorithms showed competitive performance in the between 140 and 180 iterations, FDBAGSK reached a better value at the end of the optimization process. The voltage profile in Fig. 14b

demonstrates that the optimization algorithms are successful in keeping the load bus voltage magnitudes within the specified limits.

**Case-7: Minimization of voltage stability index with both 3-DGs and HVDC at (2–16)** This case aims to optimize the voltage stability index (*L-index*). In this direction, FDBAGSK and AGSK are applied to perform the ORPF task in the modified power system including DGs and HVDC (between 2 and 16 buses). Optimized control parameters and corresponding objective function values are reported in Table 12. As can be seen from the table, the FDBAGSK result is

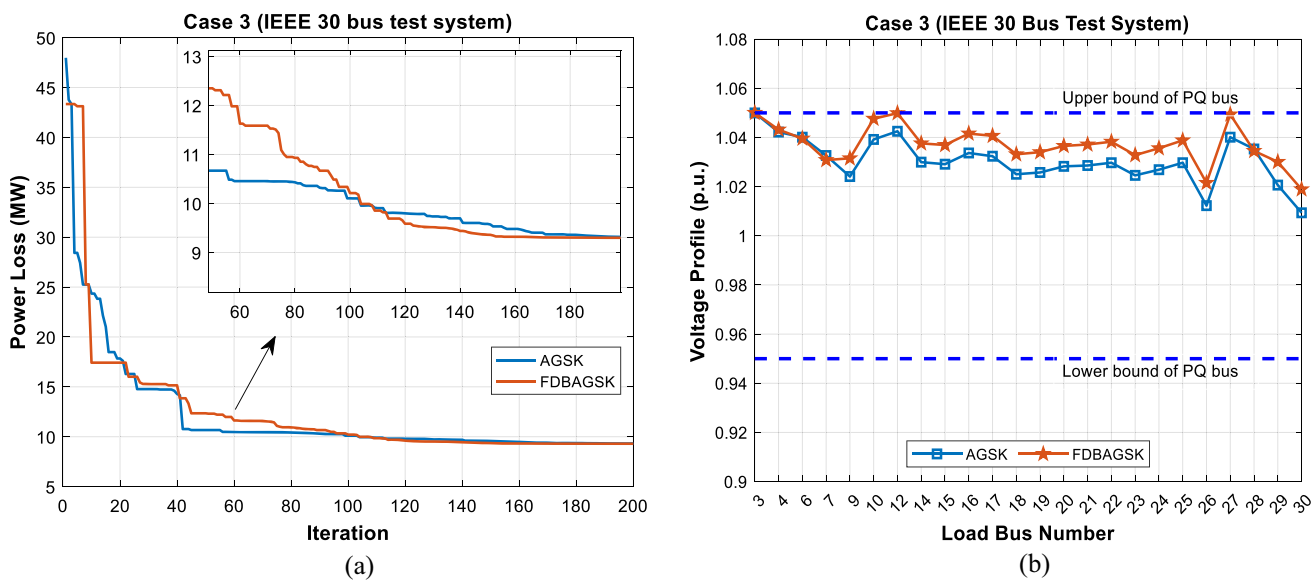


Fig. 11 Case-3: a Convergence curve of optimization algorithms, b voltage profile of load buses

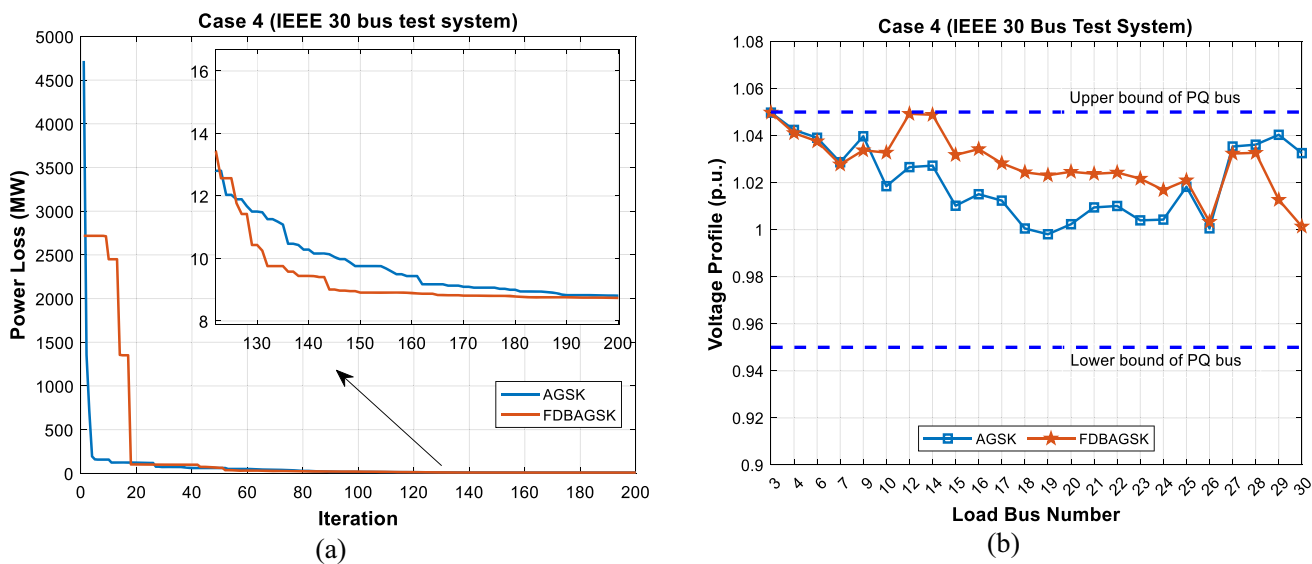


Fig. 12 Case-4: a Convergence curve of optimization algorithms, b voltage profile of load buses

0.0832 p.u., which is 2.5761% lower than that of the AGSK method. Figure 15a compares the convergence curves of the optimization algorithms. As shown in the figure, the proposed algorithm converges to the optimal solution faster than AGSK. Figure 15b reveals that the voltage values of the PQ buses are within the specified limitations.

### 5.2.2 Modified IEEE 57-bus test system

In this segment of the simulation, the effectiveness of the optimization algorithms is evaluated on the modified IEEE 57-bus power system for five test cases.

### Case-8: Minimization of active power loss with HVDC at (8–9)

Case-8 aims to reduce the active power loss of the modified IEEE 57-bus power system. For the present case, the HVDC transmission line has been added between buses 8 and 9 of the power system. Table 13 gives the optimization results achieved by FDBAGSK and basic AGSK algorithms. Accordingly, active power loss is reduced from 14.8919 MW to 13.4340 MW by using the proposed algorithm. In other words, FDBAGSK achieved a 9.7898% lower objective function value than the AGSK algorithm. Figure 16a illustrates the convergence curves of the algorithms. It can be seen from the figure that the proposed method is superior to the original AGSK in terms of solution quality and convergence

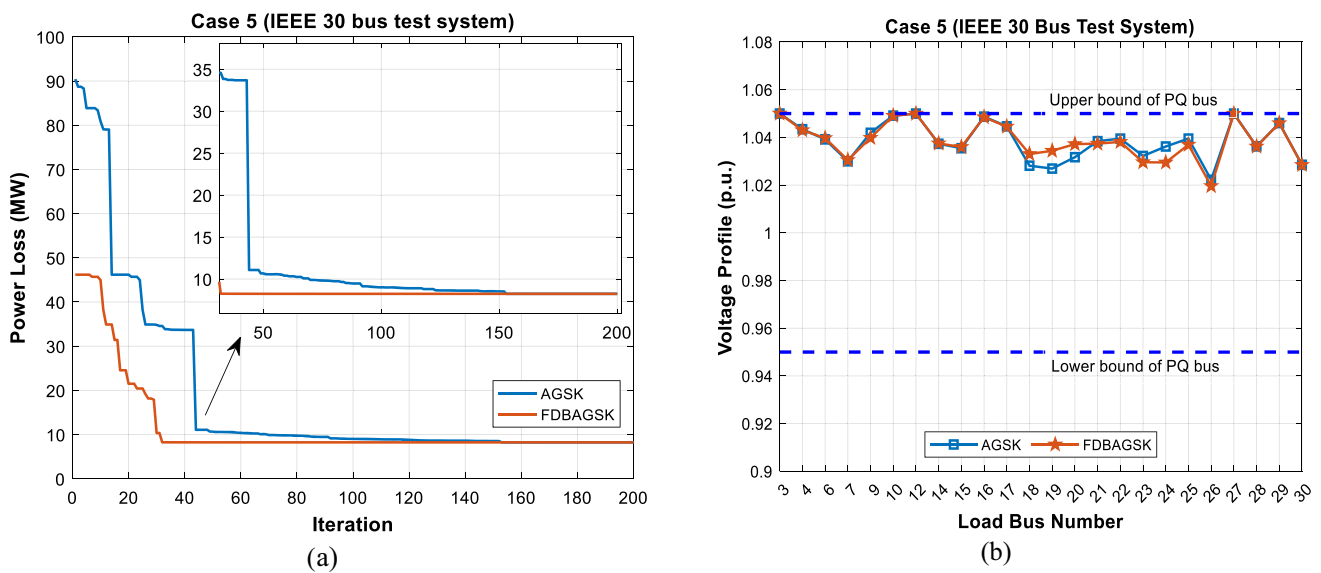


Fig. 13 Case-5: **a** Convergence curve of optimization algorithms, **b** Voltage profile of load buses

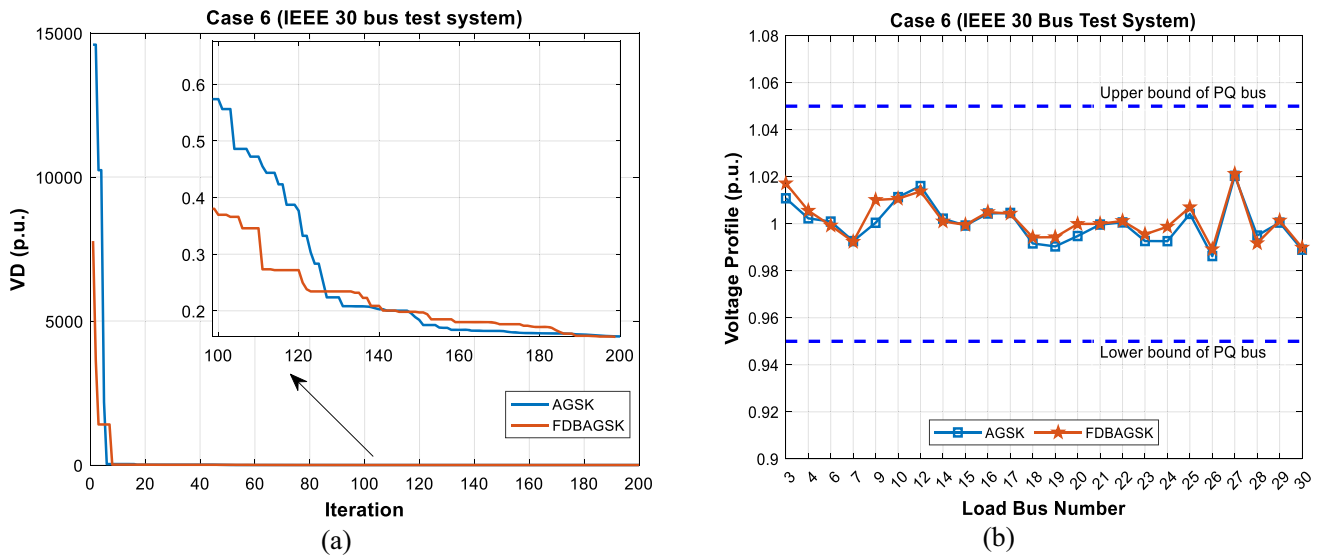


Fig. 14 Case-6: **a** Convergence curve of optimization algorithms, **b** voltage profile of load buses

speed. Figure 16b demonstrates that the voltage values of the load buses are within the specified limits (0.94–1.06 p.u.).

**Case-9: Minimization of active power loss with 3-DGs**

The objective function of this case is the minimization of active power loss considering DGs. In the present case, the location and rating of DGs are chosen as control variables. The optimized control parameters and the corresponding power loss values are summarized in Table 13. As it is evident, FDBAGSK can reach the objective function value of **9.5561 MW**, which is lower by 7.1023% compared to that of the AGSK. From the optimization results, it is observed that the solution quality of the proposed algorithm is better than the AGSK. Figure 17a shows the evolution of the fitness

value obtained by the algorithms depending on the number of iterations. We can notice from the figure, the FDBAGSK algorithm provides superiority over the basic AGSK in terms of both convergence speed and solution accuracy. As shown in Fig. 17b, all algorithms successfully satisfy the load bus voltage constraint.

**Case-10: Minimization of active power loss with both 3-DGs and HVDC at (8–9)**

This case aims to perform the ORPF task by minimizing active power loss. To this end, FDBAGSK and AGSK algorithms are applied to the solution of ORPF in the IEEE 57-bus test system incorporating DGs and HVDC (between buses 8 and 9). Table 13 summarizes the optimization results. As shown in Table 13, the FDBAGSK algorithm

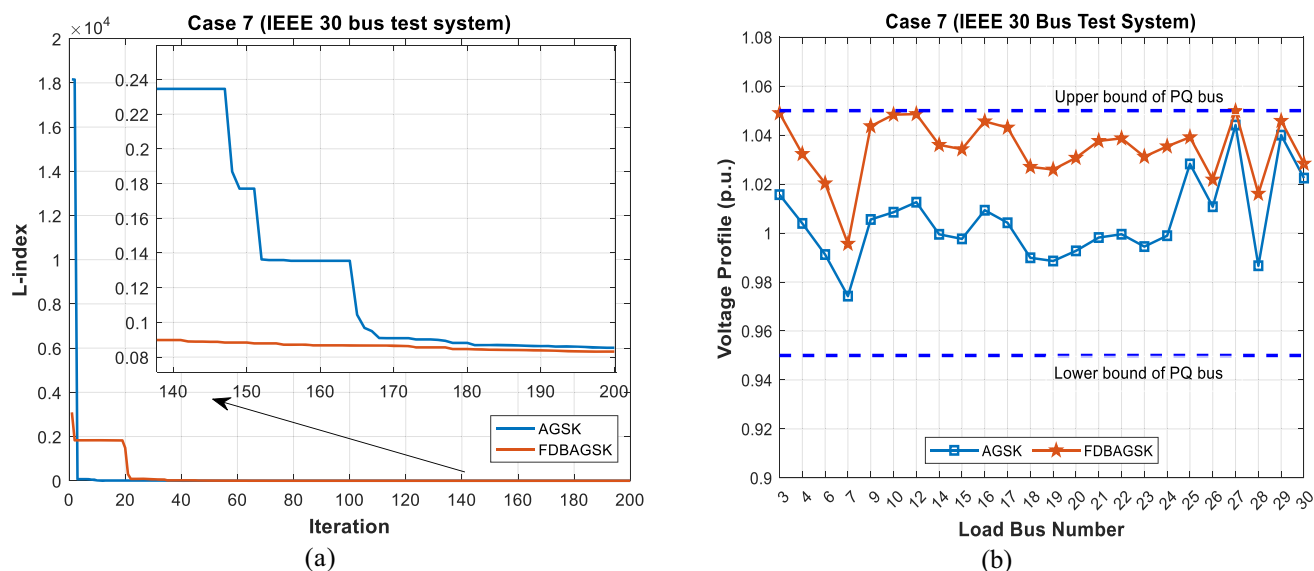


Fig. 15 Case-7: **a** Convergence curves of optimization algorithms, **b** Voltage profile of load buses

has acquired the best objective function value of **8.2632 MW**, and the objective function value is 9.0513 MW in the AGSK. The proposed algorithm reduces the active power loss by **8.7070%** compared to AGSK. Figure 18a displays the convergence characteristics of metaheuristic optimizers. As it can be seen from the figure, the developed FDBAGSK algorithm has a smooth curve with rapid convergence. Figure 18b shows that all load bus voltage magnitudes are within the limits at the end of the optimization process.

**Case-11: Minimization of voltage deviation with both 3 DGs and HVDC at (8–9)** The present test case has centered on the voltage deviation minimization of the modified IEEE 57-bus test system involving DGs and a two-terminal HVDC link between buses 8 and 9. The optimized control variables and attained voltage deviation results are given in Table 12. The minimum voltage deviation value achieved by FDBAGSK is **0.6006 p.u.** Quantitatively, the simulation result of the proposed algorithm is lower by **21.1500%** than that of the AGSK algorithm. The variations of voltage deviation values over the iterations are depicted in Fig. 19a. It is seen that the proposed algorithm is advantageous over the original AGSK algorithm with its fast convergence and solution quality. Figure 19b shows the load bus voltages corresponding to the optimized control variables. It can be seen from the figure that the load bus voltages are within the limits (0.94–1.06 p.u.). In other words, the load bus voltage inequality constraint has been successfully satisfied.

**Case-12: Minimization of voltage stability index with both 3 DGs and HVDC at (2–16)** Case-12 focuses on the optimization of the voltage stability index (*L*-index) in a modified IEEE 57-bus power system including HVDC between buses 2

and 16. Moreover, the present test case considers the optimal allocation of DGs. The optimal settings of control variables and careful *L*-index values are given in Table 13. The objective function values of the FDBAGSK and AGSK algorithms are **0.1266 p.u.** and **0.1310 p.u.**, respectively. The result of the proposed algorithm is **3.3587%** lower than that of the AGSK algorithm. From the optimization results, it is observed that the proposed algorithm attains the best competitive solution for the present case. Figure 20a depicts the convergence characteristics of the optimization algorithms. It is seen that using the proposed FDBAGSK rapid convergence performance is obtained. Figure 20b gives that the ORPF solutions obtained with the FDBAGSK and AGSK algorithms successfully met the load bus voltage constraint.

### 5.2.3 Statistical analysis and literature comparison

This subcategory presents the statistical analysis results and a literature comparison. In order to obtain sufficient and robust evidence for the statistical analysis, the algorithms are run 20 times for all test cases. Table 14 presents the minimum, mean, maximum, and standard deviation values of the simulation results obtained from 20 independent runs. As it can be seen from the table, the proposed FDBAGSK algorithm achieved the best objective function value for all ORPF cases. Based on the mean value index, it can be said that the proposed algorithm exhibited a stable and robust search performance.

Table 15 gives the results of the optimization algorithms used in the present study and of the LP[50], GA[51], ABC[52], SGA[53], BGA[53], and BSA[14] methods recently reported in the literature. The lack of comparative results for some test cases can be explained by the fact

**Table 13** Simulation results of the IEEE 57-bus test system

Parameters	Case-8		Case-9		Case-10		Case-11		Case-12	
	AGSK	FDBAGSK	AGSK	FDBAGSK	AGSK	FDBAGSK	AGSK	FDBAGSK	AGSK	FDBAGSK
$P_{THG1}$	26.9758	49.9457	25.4636	30.6104	43.0426	46.6089	24.5782	34.9153	28.7235	38.8512
$P_{THG2}$	54.6507	30.1602	63.1375	49.2122	30.3652	46.2379	82.5239	30.8265	67.5415	57.3783
$P_{THG3}$	236.9193	227.6800	149.2326	222.4564	195.1429	179.2892	361.3316	263.8426	316.7358	364.3883
$P_{THG6}$	49.5783	49.3309	49.7982	22.9807	48.4272	49.8695	34.6198	23.3795	42.3047	49.2948
$P_{THG8}$	49.8826	49.9930	48.7995	47.2963	49.8094	49.9925	30.8586	39.2736	32.1008	44.2012
$P_{THG9}$	333.2484	312.9041	340.4193	317.3585	333.5257	301.5697	233.5147	285.1528	211.3721	323.9477
$P_{THG12}$	514.4658	544.2258	511.1395	492.0636	481.2283	501.6299	446.1090	526.7780	519.4815	323.1576
$Q_{THG1}$	58.0473	37.9571	- 9.1729	60.1995	43.2363	5.4075	36.7130	35.2204	0.4565	- 4.0502
$Q_{THG2}$	25.8078	49.7940	33.0631	49.1866	45.7093	49.8226	12.8619	- 12.9930	45.2149	19.8656
$Q_{THG3}$	31.5583	49.5377	50.6560	21.7291	25.3467	46.7983	58.8217	- 6.1540	42.1675	35.6769
$Q_{THG6}$	0.1914	- 0.5602	1.0844	11.5760	- 2.1071	11.0537	3.1370	23.4644	23.5902	8.3586
$Q_{THG8}$	109.5847	89.2406	124.4702	39.3542	100.3277	63.9191	195.9794	199.7145	182.4718	193.5342
$Q_{THG9}$	8.9413	8.7863	1.2766	8.4496	6.9595	8.9787	8.6244	0.9809	6.7426	3.9631
$Q_{THG12}$	72.6754	51.5550	60.7012	68.5428	71.1931	83.7272	90.9796	153.6243	78.1393	135.6738
$V_{THG1}$	1.0540	1.0488	0.9943	1.0448	1.0443	1.0452	1.0084	0.9966	1.0400	1.0321
$V_{THG2}$	1.0474	1.0467	0.9950	1.0404	1.0395	1.0454	1.0051	0.9798	1.0427	1.0310
$V_{THG3}$	1.0576	1.0563	1.0204	1.0398	1.0447	1.0580	1.0330	1.0023	1.0629	1.0654
$V_{THG6}$	1.0376	1.0285	1.0283	1.0133	1.0290	1.0415	0.9964	1.0052	1.0427	1.0478
$V_{THG8}$	1.0504	1.0391	1.0534	1.0157	1.0421	1.0432	1.0146	1.0324	1.0521	1.0678
$V_{THG9}$	1.0487	1.0370	1.0340	1.0249	1.0388	1.0456	1.0020	1.0225	1.0392	1.0524
$V_{THG12}$	1.0642	1.0522	1.0272	1.0463	1.0539	1.0668	1.0263	1.0600	1.0628	1.0675
$T_{19}$	0.9588	1.0998	0.9858	1.0108	0.9797	0.9945	1.0110	0.9363	0.9599	1.0573
$T_{20}$	1.0496	0.9667	1.0996	1.0568	0.9576	0.9894	0.9282	0.9897	1.0393	1.0594
$T_{31}$	0.9204	1.0251	1.0176	1.0329	0.9979	0.9943	0.9552	0.9780	1.0827	0.9328
$T_{35}$	0.9178	0.9603	0.9017	0.9072	0.9087	0.9072	0.9532	0.9277	0.9194	0.9485
$T_{36}$	0.9729	0.9189	0.9019	1.0441	0.9061	0.9805	0.9271	0.9137	0.9866	1.0027
$T_{37}$	1.0302	0.9887	0.9941	0.9770	1.0082	1.0146	1.0546	1.0042	0.9727	1.0592
$T_{41}$	1.0046	0.9623	0.9931	0.9430	1.0162	1.0104	0.9530	0.9613	0.9601	1.0040
$T_{46}$	0.9308	0.9726	0.9797	0.9553	0.9440	0.9904	0.9638	0.9669	0.9622	0.9566

Table 13 (continued)

Parameters	Case-8		Case-9		Case-10		Case-11		Case-12	
	AGSK	FDBAGSK	AGSK	FDBAGSK	AGSK	FDBAGSK	AGSK	FDBAGSK	AGSK	FDBAGSK
$T_{54}$	1.0188	1.0024	0.9571	0.9433	0.9559	0.9010	0.9171	0.9870	0.9571	0.9725
$T_{58}$	0.9785	0.9775	0.9606	0.9627	1.0030	1.0014	0.9339	0.9515	0.9748	0.9737
$T_{59}$	0.9570	0.9744	0.9540	0.9647	0.9819	0.9879	0.9512	0.9753	0.9586	1.0449
$T_{65}$	0.9953	0.9878	0.9527	1.0034	1.0114	1.0234	1.0235	1.0115	1.0002	0.9601
$T_{66}$	0.9113	0.9383	0.9208	0.9296	0.9734	0.9773	0.9570	0.9566	1.0540	1.0573
$T_{71}$	0.9876	0.9585	1.0278	0.9515	0.9952	0.9806	0.9703	0.9863	0.9722	1.0047
$T_{73}$	0.9889	0.9919	0.9596	1.0745	0.9861	1.0632	1.0260	0.9642	0.9505	0.9561
$T_{76}$	0.9210	1.0583	1.0561	0.9041	1.0356	0.9347	1.0451	1.0265	1.0096	1.0239
$T_{80}$	0.9874	0.9775	0.9682	0.9652	0.9927	1.0161	0.9796	0.9784	0.9918	1.0585
$P_r$	0.3837	0.1483	-	-	0.3118	0.2120	1.0569	1.1692	0.9936	1.1071
$P_i$	0.3834	0.1483	-	-	0.3116	0.2119	1.0543	1.1660	0.9915	1.1046
$Q_r$	0.2321	0.0852	-	-	0.1878	0.0886	0.5635	0.4827	0.5348	0.4220
$Q_i$	0.1019	0.0788	-	-	0.1790	0.1092	0.4201	0.4028	0.3686	0.5156
$t_r$	1.0735	0.9299	-	-	1.0013	1.0056	0.9893	0.9287	0.9930	0.9458
$t_i$	0.9512	0.9146	-	-	0.9915	1.0411	0.9492	0.9146	0.9423	0.9874
$\alpha_r(^{\circ})$	29.6508	29.0628	-	-	29.6169	21.4632	21.9211	12.3876	23.0849	11.8598
$\gamma_i(^{\circ})$	12.7799	27.4965	-	-	29.0076	26.7058	16.9526	12.5222	15.9307	21.4155
$v_{dr}$	1.3030	1.1314	-	-	1.2071	1.3073	1.1961	1.1969	1.2423	1.2745
$v_{di}$	1.3020	1.1310	-	-	1.2062	1.3067	1.1932	1.1936	1.2396	1.2716
$i_d$	0.2945	0.1311	-	-	0.2583	0.1662	0.8836	0.9769	0.7999	0.8686
$P_{DG1}(loc_{DG1})$	-	-	22.5279 (30)	29.9009 (36)	28.1393 (35)	27.6960 (53)	20.6183 (7)	26.5791 (37)	23.7345 (31)	29.3885 (36)
$P_{DG2}(loc_{DG2})$	-	-	29.7615(56)	24.1305 (53)	26.9183 (53)	27.6424 (24)	12.6449 (24)	15.1361 (14)	3.9487 (37)	25.8985 (31)
$P_{DG3}(loc_{DG3})$	-	-	20.8071 (28)	24.3466 (24)	23.2746 (24)	28.5358 (36)	27.6998 (32)	26.9202 (34)	25.6087 (35)	19.0698 (26)
$P_{loss}(MW)$	14.8919	<b>13.4340</b>	10.2867	<b>9.5561</b>	9.0513	<b>8.2632</b>	23.4380	21.6850	20.5383	24.5240
$VD(p.u.)$	1.3751	1.3580	0.9935	1.1779	0.8773	0.9421	0.7617	<b>0.6006</b>	1.1477	1.1684
$L-index$	0.2919	0.2994	0.1661	0.2031	0.1913	0.1999	0.1628	0.2068	0.1310	<b>0.1266</b>

Bold values show the best objective function value

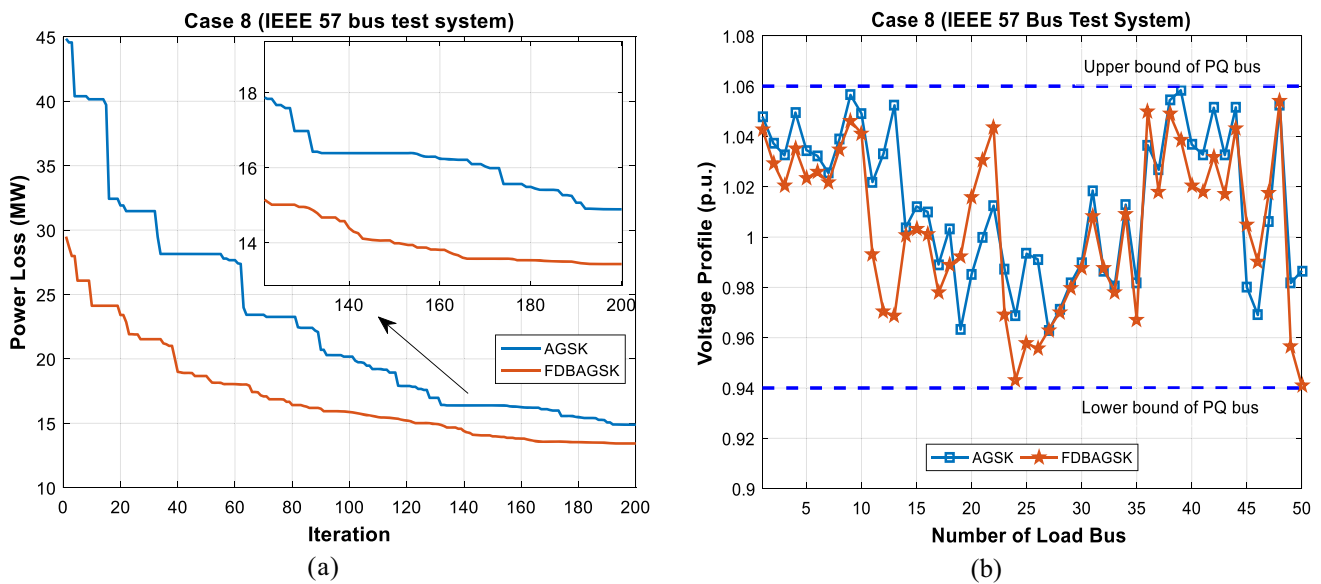


Fig. 16 Case-8: **a** Convergence curve of optimization algorithms, **b** voltage profile of load buses

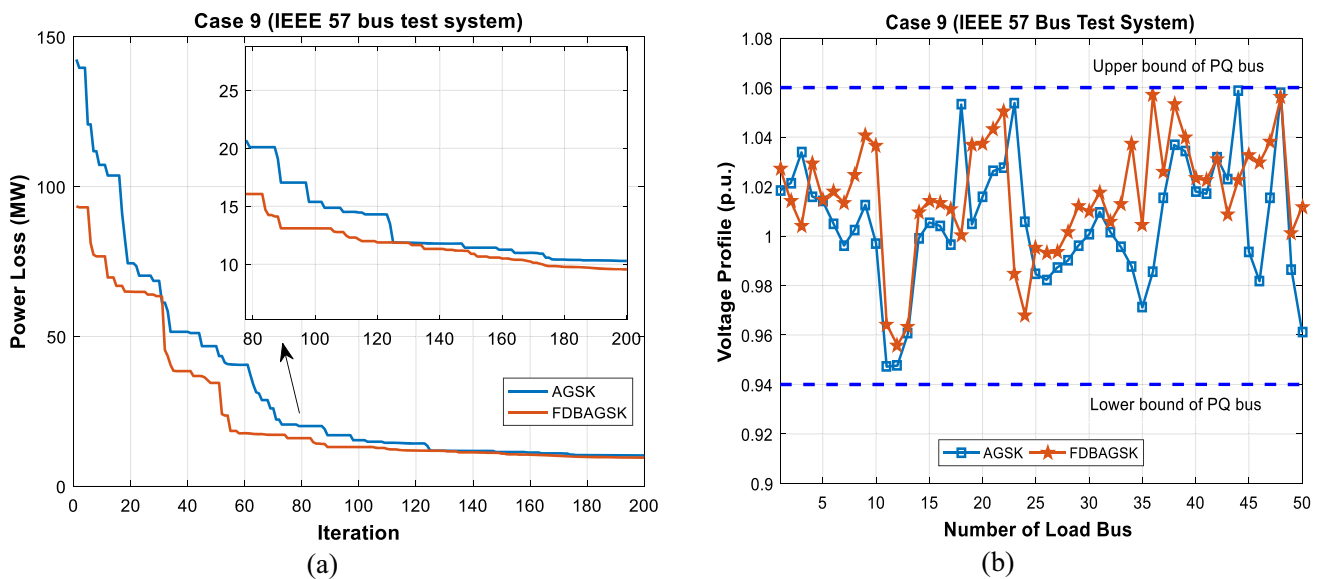


Fig. 17 Case-9: **a** Convergence curve of optimization algorithms, **b** voltage profile of load buses

that simulation studies are unique to this study. In the relevant table, the best result for each test case is highlighted in bold. Considering the experimental results obtained from the comparison of the proposed algorithm with state-of-the-art methods, it is seen that the developed FDBAGSK algorithm provides superior results in solution quality and robustness.

## 6 Conclusions

In this study, design changes were made in the search strategies of the AGSK algorithm using the FDB method and thus, the FDBAGSK was developed as a novel hybrid algorithm. The search performance of the proposed algorithm

was tested by comprehensive experimental studies. In the first stage, the performance of the proposed FDBAGSK algorithm was evaluated using 39 benchmark functions in the CEC 2017 and CEC 2020 test suites. Unimodal, multimodal, hybrid, and composition type test problems were used and the convergence accuracy of the algorithm in different sized search spaces was examined. Non-parametric Friedman and Wilcoxon test methods were applied to interpret the results obtained from the experimental studies and to unequivocally reveal the search performance of the algorithms. Statistical analysis results showed that the proposed FDBAGSK algorithm exhibits a more stable and robust search performance compared to its competitors. Moreover,

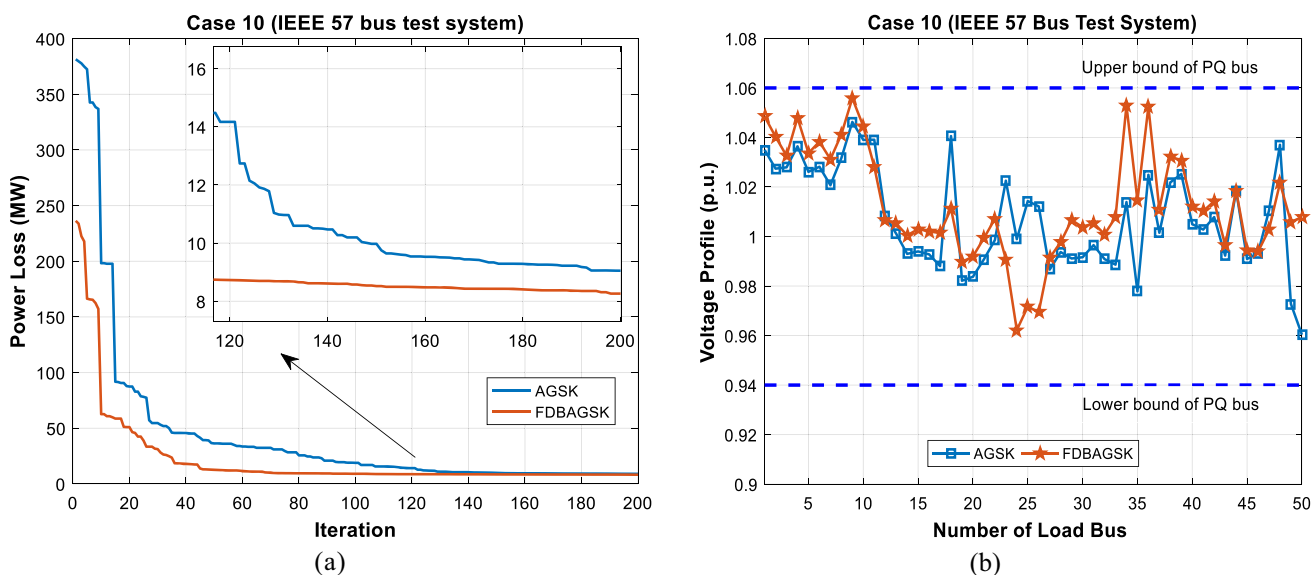


Fig. 18 Case-10: **a** Convergence curve of optimization algorithms, **b** Voltage profile of load buses

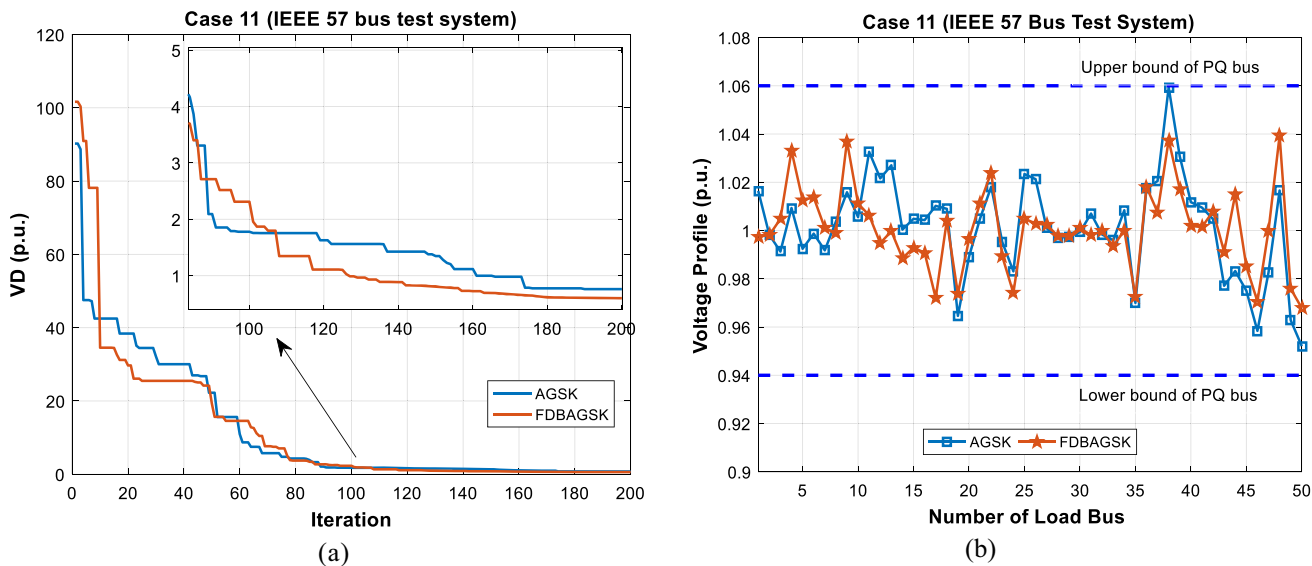


Fig. 19 Case-11: **a** Convergence curve of optimization algorithms, **b** voltage profile of load buses

the computational complexity of the AGSK and FDBAGSK algorithms were highly similar and reasonable. Although the FDB selection method added new computational processes to the FDBAGSK search-process lifecycle, the reasonable complexity achieved by the proposed algorithm is an important indicator of its usability and functionality.

The second phase of experimental studies was carried out to evaluate the search performance of the FDBAGSK on constrained real-world engineering problems. In this direction, the proposed algorithm was applied to the solution of the AC/DC-ORPF problem incorporating DGs and HVDC systems. The practicability of the FDBAGSK is investigated on

modified IEEE 30- and IEEE 57-bus test systems for the minimization of non-convex objective functions. The simulation results obtained from the FDBAGSK method for the different test cases were compared to the results of well-known optimization algorithms in the literature. From the numerical results, it is observed that the proposed algorithm achieved the best results for the optimization of the AC/DC-ORPF problem.

Source codes of the FDBAGSK algorithm (proposed method) can be accessed at this link: [https://www.mathworks.com/matlabcentral/fileexchange/129154-fdb-agsk?s\\_tid=srchtitle](https://www.mathworks.com/matlabcentral/fileexchange/129154-fdb-agsk?s_tid=srchtitle).

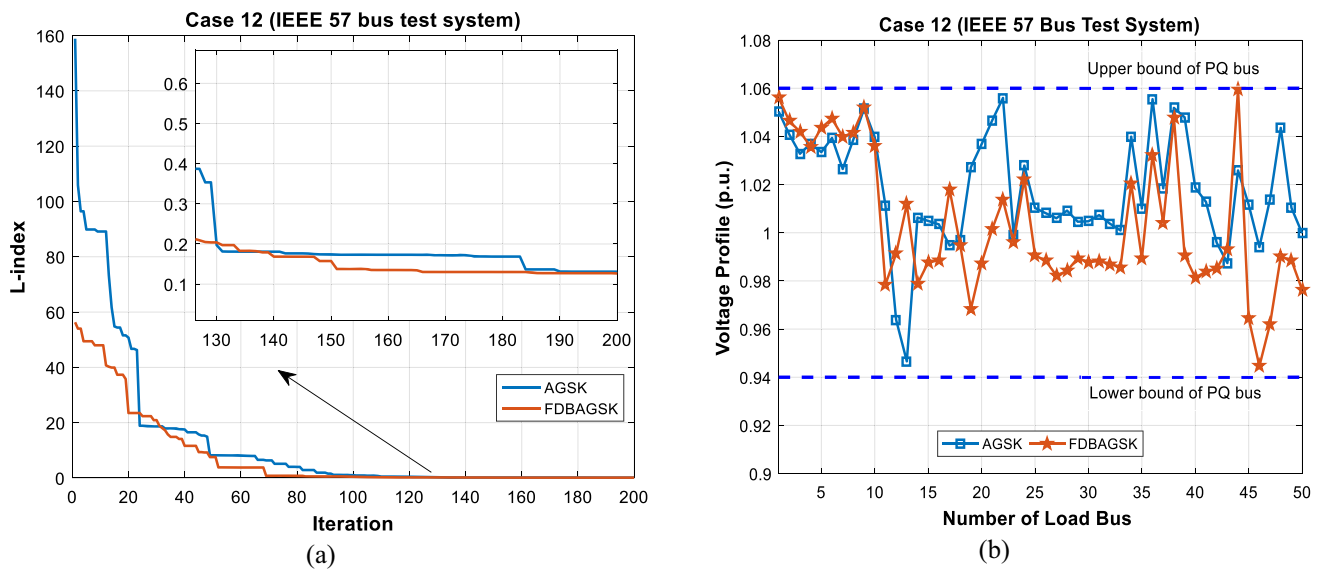


**Fig. 20** Case-12: **a** Convergence curves of algorithms, **b** voltage profile of load buses

**Table 14** Simulation results obtained from 20 independent runs

Methods	IEEE 30-bus test system						
	Case-1	Case-2	Case-3	Case-4	Case-5	Case-6	Case-7
<i>FDBAGSK</i>							
Min	11.4208	11.0921	9.2984	8.7366	8.2344	0.1539	0.0832
Mean	12.0379	11.6414	9.4229	10.1059	8.2766	0.2495	0.1433
Max	14.3864	12.9122	9.5521	13.6128	8.3650	0.5407	0.3794
Std	0.7591	0.5999	0.0688	1.1609	0.0319	0.1206	0.0740
<i>AGSK</i>							
Min	11.5165	11.1171	9.3182	8.8093	8.2391	0.1548	0.0854
Mean	12.1538	12.5290	9.4248	10.2461	8.2739	0.2947	0.1436
Max	14.2305	20.1886	9.5283	12.9387	8.3943	0.7886	0.3860
Std	0.6253	2.5484	0.0578	0.9910	0.0348	0.1776	0.0745
Methods	IEEE 57-bus test system						
	Case-8	Case-9	Case-10	Case-11	Case-12		
<i>FDBAGSK</i>							
Min	13.4340	9.5561	8.2632	0.6006	0.1266		
Mean	17.0629	11.3552	10.0639	1.052	0.2580		
Max	19.4729	13.8341	12.2768	1.5083	0.7655		
Std	1.4734	1.0795	0.9755	0.2848	0.1729		
<i>AGSK</i>							
Min	14.8919	10.2867	9.0513	0.7617	0.1310		
Mean	17.5297	12.3759	10.4778	1.3096	0.4181		
Max	20.5611	16.2046	11.8339	2.6985	1.3138		
Std	1.6504	1.7442	0.8927	0.4616	0.2968		

**Table 15** Comparison with results in the literature

IEEE 30-bus test system							
Methods	Case-1	Methods	Case-2	Methods	Case-3	Methods	Case-4
LP [50]	28.41 MW	LP [50]	12.01 MW	SGA [53]	14.1317 MW	ABC [52]	8.9172 MW
GA [51]	12.40 MW	GA [51]	12.01 MW	BGA [53]	13.9888 MW	BSA [14]	8.8525 MW
ABC [52]	11.6783 MW	ABC [52]	11.4767 MW	ABC [52]	9.4248 MW	AGSK	8.8093 MW
BSA [14]	11.5339 MW	BSA [14]	11.2483 MW	BSA [14]	9.3039 MW	FDBAGSK	<b>8.7366 MW</b>
AGSK	11.5165 MW	AGSK	11.1171 MW	AGSK	9.3182 MW		
FDBAGSK	<b>11.4208 MW</b>	FDBAGSK	<b>11.0921 MW</b>	FDBAGSK	<b>9.2984 MW</b>		
Methods	Case-5	Methods	Case-6	Methods	Case-7	Methods	Case-7
ABC [52]	8.8032 MW	AGSK	0.1548 p.u	AGSK	0.0854 p.u		
AGSK	8.2391 MW	FDBAGSK	<b>0.1539 p.u</b>	FDBAGSK	<b>0.0832 p.u</b>		
FDBAGSK	8.2344 MW						
BSA [14]	<b>8.2080 MW</b>						
IEEE 57-bus test system							
Methods	Case-8	Methods	Case-9	Methods	Case-10	Methods	Case-11
GA [14]	14.2370 MW	GA [14]	13.8188 MW	AGSK	9.0513 MW	AGSK	0.7614 p.u
BSA [14]	14.0607 MW	BSA [14]	11.8235 MW	GA [14]	9.0152 MW	FDBAGSK	<b>0.6006 p.u</b>
AGSK	14.8919 MW	AGSK	10.2867 MW	BSA [14]	8.4060 MW		
FDBAGSK	<b>13.4340 MW</b>	FDBAGSK	<b>9.5561 MW</b>	FDBAGSK	<b>8.2632 MW</b>		
Methods	Case-12	Methods	Case-12	Methods	Case-12	Methods	Case-12
AGSK							0.1310 p.u
FDBAGSK							<b>0.1266 p.u</b>

Bold values show the best objective function value

**Acknowledgements** Hüseyin Bakır would like to thank the support provided by Scientific and Technological Research Council of Turkey (TUBITAK) BİDEB 2211/A National PhD Scholarship Program under application number 1649B031806288.

## References

- Abaci K, Yamaçlı V (2017) Optimal reactive-power dispatch using differential search algorithm. *Electr Eng* 99(1):213–225
- Nguyen TT, Vo DN (2020) Improved social spider optimization algorithm for optimal reactive power dispatch problem with different objectives. *Neural Comput Appl* 32(10):5919–5950
- Yalçın E, Çam E, Taplamacıoğlu MC (2020) A new chaos and global competitive ranking-based symbiotic organisms search algorithm for solving reactive power dispatch problem with discrete and continuous control variable. *Electr Eng* 102(2):573–590
- Ayan K, Kılıç U (2012) Artificial bee colony algorithm solution for optimal reactive power flow. *Appl Soft Comput* 12(5):1477–1482
- Yalçın F, Arifoğlu U (2013) A new approach based on genetic algorithm for optimal reactive power flow solution in multi-terminal AC-DC systems. *Przeglad Elektrotechniczny* 89(3a):231–235
- Moghadam A, Seifi AR (2014) Fuzzy-TLBO optimal reactive power control variables planning for energy loss minimization. *Energy Convers Manage* 77:208–215
- Sulaiman MH, Mustafa Z, Mohamed MR, Aliman O (2015) Using the gray wolf optimizer for solving optimal reactive power dispatch problem. *Appl Soft Comput* 32:286–292
- Mehdinejad M, Mohammadi-Ivatloo B, Dadashzadeh-Bonab R, Zare K (2016) Solution of optimal reactive power dispatch of power systems using hybrid particle swarm optimization and imperialist competitive algorithms. *Int J Electr Power Energy Syst* 83:104–116
- Lenin K, Reddy BR, Suryakalavathi M (2016) Hybrid Tabu search-simulated annealing method to solve optimal reactive power problem. *Int J Electr Power Energy Syst* 82:87–91
- Mei RNS, Sulaiman MH, Mustafa Z, Daniyal H (2017) Optimal reactive power dispatch solution by loss minimization using moth-flame optimization technique. *Appl Soft Comput* 59:210–222
- Sakr WS, El-Sehiemy RA, Azmy AM (2017) Adaptive differential evolution algorithm for efficient reactive power management. *Appl Soft Comput* 53:336–351
- ben oualid Medani, K., Sayah, S., & Bekrar, A. (2018) Whale optimization algorithm based optimal reactive power dispatch: a case study of the Algerian power system. *Electric Power Syst Res* 163:696–705
- Shaheen MA, Yousri D, Fathy A, Hasanien HM, Alkuhayli A, Muyeen SM (2020) A novel application of improved marine predators

- algorithm and particle swarm optimization for solving the ORPD problem. *Energies* 13(21):5679
14. Fadel W, Kilic U, Ayan K (2021) Optimal reactive power flow of power systems with two-terminal HVDC and multi distributed generations using backtracking search algorithm. *Int J Electrical Power Energy Syst*, 127, 106667.
  15. Radosavljević J (2018) Metaheuristic optimization in power engineering. *Institution of Engineering and Technology*
  16. Naderi E, Narimani H, Pourakbari-Kasmaei M, Cerna FV, Marzband M, Lehtonen M (2021) State-of-the-art of optimal active and reactive power flow: a comprehensive review from various standpoints. *Processes* 9(8):1319
  17. Wei Y, Zhou Y, Luo Q, Deng W (2021) Optimal reactive power dispatch using an improved slime mould algorithm. *Energy Rep* 7:8742–8759
  18. Duman S, Li J, Wu L, Guvenc U (2019). Optimal power flow with stochastic wind power and FACTS devices: a modified hybrid PSO-GSA with chaotic maps approach. *Neural Comput Appl* 1–30
  19. Vidyasagar S, Vijayakumar K, Sattianadan D, Fernandez SG (2016) Optimal placement of DG based on voltage stability index and voltage deviation index. *Indian J Sci Technol*, 9(38)
  20. Duman S, Li J, Wu L, Yorukeren N (2021) Symbiotic organisms search algorithm-based security-constrained AC–DC OPF regarding uncertainty of wind, PV and PEV systems. *Soft Comput* 1–38
  21. Chaib AE, Bouchekara HREH, Mehasni R, Abido MA (2016) Optimal power flow with emission and non-smooth cost functions using backtracking search optimization algorithm. *Int J Electr Power Energy Syst* 81:64–77
  22. Duman S (2018) A modified moth swarm algorithm based on an arithmetic crossover for constrained optimization and optimal power flow problems. *IEEE Access* 6:45394–45416
  23. Pulluri H, Naresh R, Sharma V (2017) An enhanced self-adaptive differential evolution based solution methodology for multiobjective optimal power flow. *Appl Soft Comput* 54:229–245
  24. Ayan K, Kiliç U (2016) Optimal power flow of two-terminal HVDC systems using backtracking search algorithm. *Int J Electr Power Energy Syst* 78:326–335
  25. Kiliç U, Ayan K (2014) Optimal power flow solution of two-terminal HVDC systems using genetic algorithm. *Electr Eng* 96(1):65–77
  26. Kiliç U, Ayan K (2013) Optimizing power flow of AC–DC power systems using artificial bee colony algorithm. *Int J Electr Power Energy Syst* 53:592–602
  27. Tong H, Zhu Y, Pierezan J, Xu Y, dos Santos Coelho L (2021) Chaotic coyote optimization algorithm. *J Ambient Intell Hum Comput* 1–21
  28. Salgotra R, Singh U, Saha S (2018) New cuckoo search algorithms with enhanced exploration and exploitation properties. *Expert Syst Appl* 95:384–420
  29. Stanovov S, Akhmedova E (2019) Semenkin, selective pressure strategy in differential evolution: exploitation improvement in solving global optimization problems. *Swarm Evol Comput* 50:100463
  30. Sörensen K (2015) Metaheuristics—the metaphor exposed. *Int Trans Oper Res* 22(1):3–18
  31. Abd Elaziz M, Yousri D, Mirjalili S (2021) A hybrid Harris hawks-moth-flame optimization algorithm including fractional-order chaos maps and evolutionary population dynamics. *Adv Eng Softw* 154:102973
  32. Dehkordi AA, Sadiq AS, Mirjalili S, Ghafoor KZ (2021) Nonlinear-based chaotic harris hawks optimizer: algorithm and internet of vehicles application. *Appl Soft Comput* 107574
  33. Aras S, Gedikli E, Kahraman HT (2021) A novel stochastic fractal search algorithm with fitness-distance balance for global numerical optimization. *Swarm Evol Comput* 61:100821
  34. Gupta S, Abderazek H, Yıldız BS, Yıldız AR, Mirjalili S, Sait SM (2021) Comparison of metaheuristic optimization algorithms for solving constrained mechanical design optimization problems. *Exp Syst Appl* 115351
  35. Halim AH, Ismail I, Das S (2020). Performance assessment of the metaheuristic optimization algorithms: an exhaustive review. *Artif Intell Rev*, 1–87
  36. Turkeš R, Sörensen K, Hvattum LM (2021) Meta-analysis of metaheuristics: quantifying the effect of adaptiveness in adaptive large neighborhood search. *Eur J Oper Res* 292(2):423–442
  37. Kahraman HT, Aras S, Gedikli E (2020) Fitness-distance balance (FDB): a new selection method for meta-heuristic search algorithms. *Knowl-Based Syst* 190:105169
  38. Bakir H, Guvenc U, Kahraman HT, Duman S (2022) Improved Lévy flight distribution algorithm with FDB-based guiding mechanism for AVR system optimal design. *Comput Ind Eng* 168:108032
  39. Kahraman HT, Bakir H, Duman S, Katı M, Aras S, Guvenc U (2022) Dynamic FDB selection method and its application: modeling and optimizing of directional overcurrent relays coordination. *Appl Intell* 52(5):4873–4908
  40. Mohamed AW, Hadi AA, Mohamed AK, Awad NH (2020) Evaluating the performance of adaptive GainingSharing knowledge based algorithm on CEC 2020 benchmark problems. In: 2020 IEEE congress on evolutionary computation (CEC), pp 1–8. IEEE.
  41. Mohamed AW, Hadi AA, Mohamed AK (2019) Gaining-sharing knowledge based algorithm for solving optimization problems: a novel nature-inspired algorithm. *Int J Mach Learn Cybernet*, 1–29
  42. Derrac J, García S, Molina D, Herrera F (2011) A practical tutorial on the use of nonparametric statistical tests as a methodology for comparing evolutionary and swarm intelligence algorithms. *Swarm. Evol Comput* 1:3–18
  43. García S, Fernández A, Luengo J, Herrera F (2010) Advanced nonparametric tests for multiple comparisons in the design of experiments in computational intelligence and data mining: Experimental analysis of power. *Inform Sci* 180(10):2044–2064
  44. Awad NH, Ali MZ, Liang JJ, Qu BY, Suganthan PN (2016) Problem definitions and evaluation criteria for the CEC 2017 special session and competition on single objective real-parameter numerical optimization.”, Technical Report, 2016
  45. Yue CT, Price KV, Suganthan PN, Liang JJ, Ali MZ, Qu BY, Awad NH, Biswas PP (2019) Problem definitions and evaluation criteria for the CEC 2020 special session and competition on single objective bound constrained numerical optimization. *Tech. Rep.*, Zhengzhou University and Nanyang Technological University, 2019
  46. Liang JJ, Qu BY, Suganthan PN (2013) Problem definitions and evaluation criteria for the CEC 2014 special session and competition on single objective real-parameter numerical optimization. *Zhengzhou University, Zhengzhou China and Technical Report*, Nanyang Technological University, Singapore, Computational Intelligence Laboratory
  47. MATPOWER <http://www.pserc.cornell.edu/matpower/>.
  48. IEEE 30-bus test system data [http://labs.ece.uw.edu/pstca/pf30/pg\\_tca30bus.htm](http://labs.ece.uw.edu/pstca/pf30/pg_tca30bus.htm)
  49. IEEE 57-bus test system data [http://labs.ece.uw.edu/pstca/pf57/pg\\_tca57bus.htm](http://labs.ece.uw.edu/pstca/pf57/pg_tca57bus.htm)
  50. Taghavi R, Seifi A (2012) Optimal reactive power control in hybrid power systems. *Electr Power Compon Syst* 40(7):741–758
  51. Kiliç U, Ayan K, Arifoğlu U (2014) Optimizing reactive power flow of HVDC systems using genetic algorithm. *Int J Electr Power Energy Syst* 55:1–12
  52. Kiliç U, Ayan K (2016) Artificial bee colony algorithm based optimal reactive power flow of two-terminal HVDC systems. *Turk J Electr Eng Comput Sci* 24(3):1075–1090

53. Yusran Y (2014) Electrical network power quality improvement through distributed generation optimum placement based on breeder genetic algorithm method. In: The international on electrical engineering and informatics conference (MICEEI), Makassar, South Sulawesi, Indonesia; 2014. pp 26–30
- Springer Nature or its licensor (e.g. a society or other partner) holds exclusive rights to this article under a publishing agreement with the author(s) or other rightsholder(s); author self-archiving of the accepted manuscript version of this article is solely governed by the terms of such publishing agreement and applicable law.

**Publisher's Note** Springer Nature remains neutral with regard to jurisdictional claims in published maps and institutional affiliations.